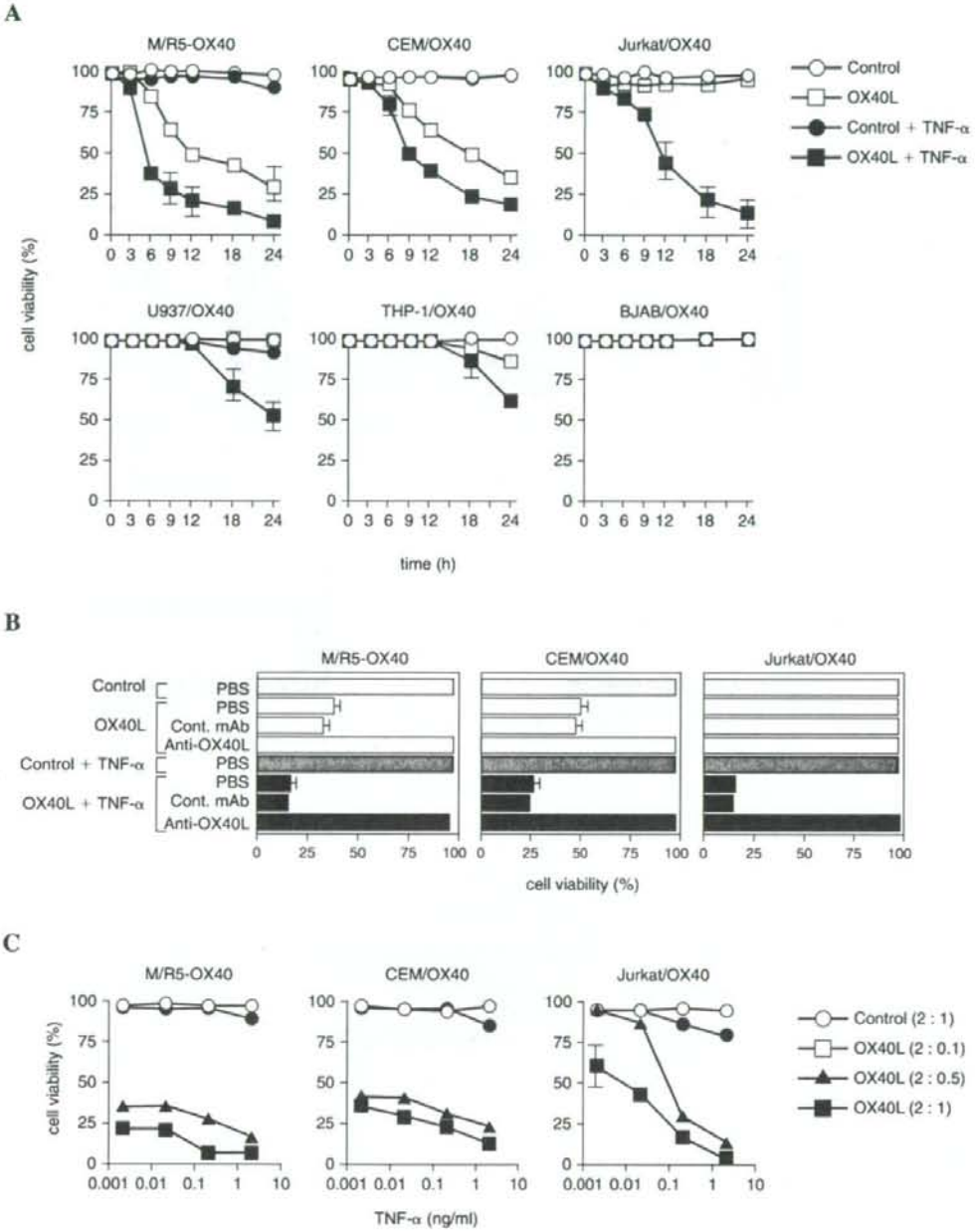

FIG. 3. Cell type-dependent induction of cell death by stimulation with OX40L alone or by combined activation with OX40L and TNF. Cell viability was determined by an eosin-Y dye exclusion assay, 24 h after stimulation by coculture with PFA-fixed SV-T2/OX40L (OX40L) or with PFA-fixed SV-T2/control (Control) cells in the presence or absence of TNF-α (2 ng/ml or graded concentrations). (**A**) The three $CD4^+$ T cell lines, Molt-4/CCR5-OX40 (M/R5-OX40), CEM/OX40, and Jurkat/OX40, the two promonocytic cell lines U937/OX40 and THP-1/OX40, and the B cell lines BJAB/OX40 were examined. (**B**) The blocking effect of anti-hOX40L mAb (Anti-OX40L, 10 μg/ml) on cell death of OX40-expressing $CD4^+$ T cell lines was determined. (**C**) The cell death of OX40-expressing $CD4^+$ T cell lines was induced by the addition of various concentrations of TNF-α, up to 2 ng/ml, and by various ratios of stimulator to responder cell. Data presented are the mean values ± SD of triplicate determinations. Representative results from three independent experiments are shown.

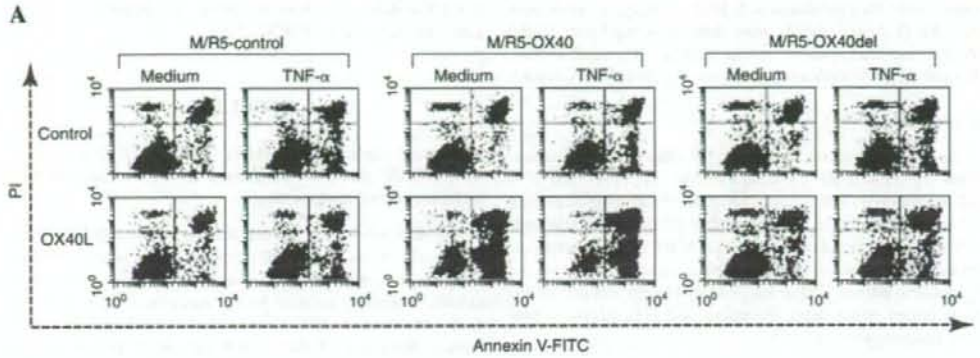
A
M/R5-control
M/R5-OX40
M/R5-OX40del
Medium
TNF-α
Control
OX40L
PI
Annexin V-FITC

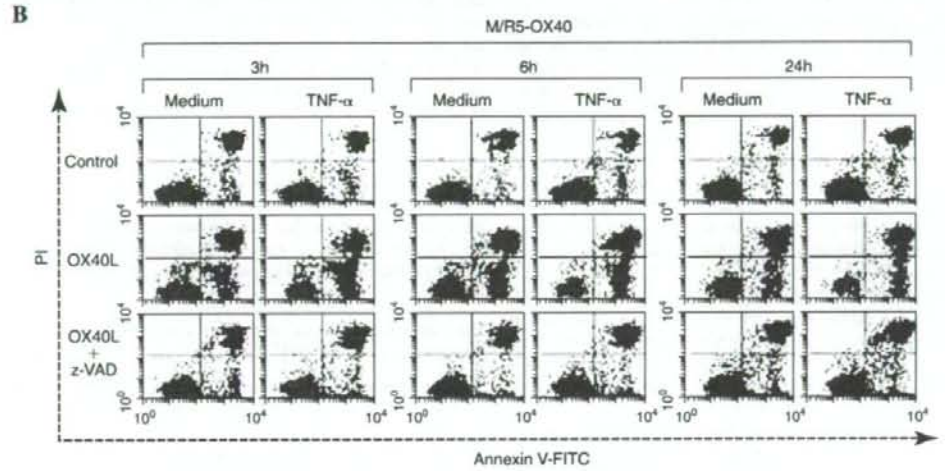
B
M/R5-OX40
3h
6h
24h
Medium
TNF-α
Control
OX40L
OX40L + z-VAD
PI
Annexin V-FITC

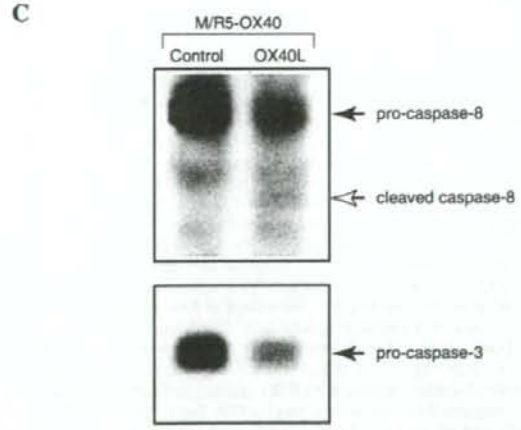
C
M/R5-OX40
Control
OX40L
pro-caspase-8
cleaved caspase-8
pro-caspase-3

branes were then incubated with HRPO-conjugated antimouse IgG Ab (1:2000). Signals were detected using Super Signal West Femto Maximum Sensitivity Substrate (Pierce, Rockford, IL) and the LAS-3000 image analyzer (Fujifilm, Tokyo, Japan).

TNF-α assay

As described above, cells (4×10^5 cells/well) were stimulated by PFA-fixed SV-T2/OX40L or by PFA-fixed SV-T2/control cells (2×10^5 cells/well), for the times indicated, in 12-well plates. For the determination of TNF-α production, culture supernatants and cell lysates ($5\text{-}6 \times 10^6$ cells/ml) were collected, and the concentrations of TNF-α were assayed using the Quantikine human TNF-α kit (R&D). The protein concentrations in cell lysates were determined using the advanced protein assay reagent.

Detections of apoptosis in primary T cells

Human peripheral blood mononuclear cells (PBMCs) were isolated from heparinized (5 U/ml) blood of normal healthy donors using standard density gradient centrifugation and a human lymphocyte separation medium (Sigma). The cells at the interface were collected and washed three times in PBS containing 2% FCS. PBMCs were resuspended at 1×10^6 cells/ml in RPMI medium, supplemented with 20 U/ml rhIL-2. Each well of 12-well plates was coated with 5 μg/ml anti-hCD3 mAb (clone OKT-3) for 1 h at 37°C and washed three times in PBS. Then, 1 ml of the cell suspension was dispensed into individual wells and cultured in the presence of either rhIL-12 or rhIL-4 at 20 ng/ml for 3 days at 37°C in a 5% CO_2 humidified incubator. The activated cells were harvested, adjusted to 2×10^5 cells/ml, and further stimulated using the same conditions at days 3 and 6. Activated PBMCs were harvested on day 9, in 20 U/ml rhIL-2-containing RPMI medium, and were then cocultivated for 24 h with either PFA-fixed SV-T2/OX40L or with PFA-fixed SV-T2/control cells at a cell to cell ratio of 1:1. Anti-hOX40L mAb (5A8) was added at 20 μg/ml to prevent OX40–OX40L interaction. The cells were then stained by Cy5-labeled anti-hCD4 mAb (OKT-4) followed by FITC-labeled annexin V to detect apoptosis. Apoptotic cells in the $CD4^+$ T cell gate were detected by FACSCalibur.

RESULTS

Combined stimulation of ACH-2/OX40 cell line cells with OX40L and TNF decreases HIV-1 production by inducing rapid apoptosis

We have previously reported that the chronically HIV-1-infected cell line ACH-2/OX40 produces large amounts of HIV-1 within 24 h, following stimulation by either coculture with OX40L-expressing cells or by the addition of TNF-α or -β. Such activation of HIV-1 replication is mediated primarily through activation of the NF-κB pathway.[38] In the present study, we examined the effect of dual stimulation by OX40L and TNF-α (or TNF-β, data not shown) on HIV-1 production. In contrast to the previously documented increase in HIV-1 production by activation via the ligation of either OX40 or TNF-R alone, dual stimulation of these two receptors resulted in a marked reduction of HIV-1 production in ACH-2/OX40 cells (Fig. 1A). The morphology of the ACH-2/OX40 cells was markedly altered following 24 h of dual stimulation (Fig. 1B). This morphological effect was associated with the induction of rapid apoptosis, as determined by apparent cell death (Fig. 1C) and by annexin V-FITC/PI staining (Fig. 1D). Of interest was the finding that all the dual receptor-stimulated ACH-2/OX40 cells became apoptotic as early as 9 h after stimulation, before HIV-1 production was detectable (Fig. 1A and D).

Dual receptor-induced activation also affects HIV-1 production in other HIV-1-infected cell line cells

To determine whether this HIV-1 reduction and this rapid cell death, induced by such dual receptor activation, were unique to the ACH-2/OX40 cells or whether they are general for all types of HIV-1-infected cells expressing these two receptors, a series of other HIV-1 productively or chronically in-

FIG. 4. Involvement of the OX40 cytoplasmic tail and of the caspase cascade in the induction of apoptosis of Molt-4/CCR5-OX40 cells. (**A**) Molt-4/CCR5-OX40 (M/R5-OX40), Molt-4/CCR5-OX40del (M/R5-OX40del), and Molt-4/CCR5-control (M/R5-control) cells were cocultured with PFA-fixed SV-T2/OX40L (OX40L) or with PFA-fixed SV-T2/control (Control) cells, at a cell-to-cell ratio of 2:1 in the absence (Medium) or in the presence of 2 ng/ml TNF-α for 24 h. (**B**) The blocking of apoptosis of the M/R5-OX40 cells, induced by OX40L or by OX40L/TNF-α stimulation, by a caspase inhibitor, z-VAD-fmk. The caspase inhibitor z-VAD-fmk (z-VAD) was added, before stimulation, to M/R5-OX40 cells at a final concentration of 100 μM. The pretreated M/R5-OX40 cells were cocultured with PFA-fixed SV-T2/OX40L (OX40L) or with PFA-fixed SV-T2/control (Control) cells, at a cell-to-cell ratio of 2:1 in the absence (Medium) or in the presence of 2 ng/ml TNF-α for 3, 6, and 24 h. Apoptotic and live cells were determined by a standard dual staining method using annexin V-FITC and PI. The cells were classified as undamaged cells, annexin V(−)/PI(−); early apoptotic cells, annexin V(+)/PI(−); and late apoptotic cells and necrotic cells, annexin V(+)/PI(+). The stimulating cells, which included the PFA-fixed SV-T2/OX40L or SV-T2/control cells, were included within the region of annexin V(+)/PI(+) cells (about 20% of the total cell number). The percentage of live cells is shown at the lower left quadrangle of each dot plot. (**C**) The cell lysates obtained from the M/R5-OX40 cells stimulated by PFA-fixed SV-T2/OX40L (OX40L) or by PFA-fixed SV-T2/control (Control) cells, at a cell-to-cell ratio of 2:1 for 6 h, were treated with an equal volume of 2× sample buffer without 2-mercaptoethanol, separated by SDS–PAGE, using a 12.5% gel, and then transferred to Immobilon-P Transfer Membrane. After blocking, the membranes were incubated with the primary anticaspase-8 and anti-caspase-3 mAbs (1:1000) followed by horseradish peroxidase-conjugated antimouse IgG Ab (1:2000). The reaction was detected using Super Signal West Femto Maximum Sensitivity Substrate and an image analyzer. Representative results from three independent experiments are shown.

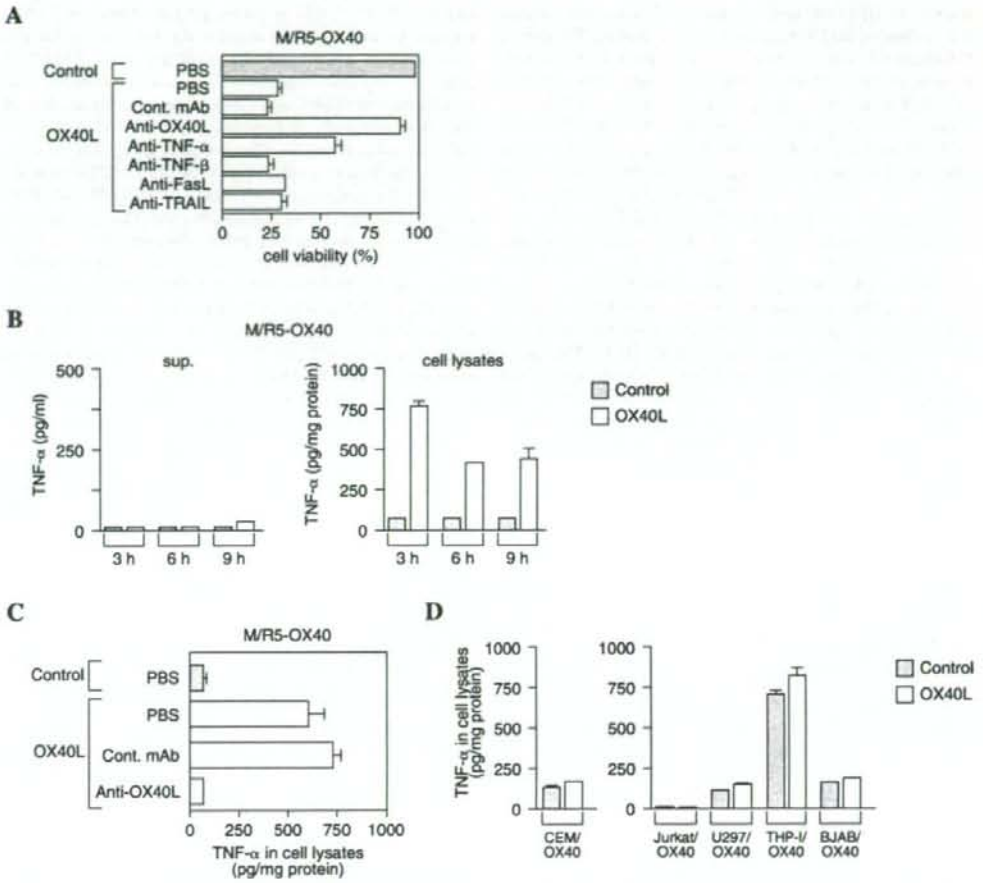

FIG. 5. OX40-induced apoptosis in Molt-4/CCR5-OX40 cells is mediated by endogenous TNF-α. (**A**) Molt-4/CCR5-OX40 (M/R5-OX40) cells were stimulated by PFA-fixed SV-T2/OX40L (OX40L) or by PFA-fixed SV-T2/control (Conrol) cells in the presence or in the absence of anti-hTNF-α (Anti-TNF-α, 30-100 μg/ml), anti-hTNF-β (Anti-TNF-β, 100 μg/ml), anti-hTRAIL (Anti-TRAIL, 100 μg/ml), anti-hFasL (Anti-FasL, 100 μg/ml), and anti-hOX40L (Anti-OX40L, 10 μg/ml) neutralizing mAb or with isotype control (Cont. mAb) for 24 h. Live cells were determined by annexin V-FITC/PI staining, followed by FACS analysis. (**B**) M/R5-OX40 cells were stimulated for 3, 6, and 9 h by PFA-fixed SV-T2/OX40L (OX40L) or by PFA-fixed SV-T2/control (Control) cells. TNF-α concentrations were determined in the culture supernatants (sup., left panel) and in the cell lysates (cell lysates, right panel) by an hTNF-α sandwich ELISA. (**C**) M/R5-OX40 cells were stimulated by PFA-fixed SV-T2/OX40L (OX40L) or by PFA-fixed SV-T2/control (Control) cells in the presence or in the absence of anti-hOX40L neutralizing mAb (Anti-OX40L, 10 μg/ml) or with isotype control (Cont. mAb) for 6 h. TNF-α concentrations were determined in the cell lysates. (**D**) The cells were stimulated by PFA-fixed SV-T2/OX40L (OX40L) or by PFA-fixed SV-T2/control (Control) cells for 6 h, in the case of CEM/OX40 cells, and for 24 h in all other cells. TNF-α concentrations were determined in the culture supernatants and in the cell lysates. The data presented are the mean values $\pm$ SD of triplicate determinations. Representative results from three independent experiments are shown.

fected cell lines transfected with OX40 were examined. These cell lines included the OX40-transfected T cell line, Molt-4/IIIB, Molt-4/IIIB-OX40 (M/IIIB-OX40), and the promonocytic cell line, U1, U1/OX40. The M/IIIB-OX40 cells produced relatively large amounts of HIV-1 upon stimulation with either OX40L or with TNF-α. The U1/OX40 cells produced significant levels of HIV-1 following stimulation with TNF-α, but produced little following ligation using OX40L. On the other hand, dual receptor activation with OX40L and TNF-α dramatically reduced HIV-1 production in M/IIIB-OX40 and in U1/OX40 cells, similar to our findings using ACH-2/OX40 cells (Fig. 2A). In M/IIIB-OX40 cells, moderate cell death was observed following OX40L stimulation, while dual stimulation, with OX40L and TNF-α, induced rapid cell death (data not

shown). In U1/OX40 cells, moderate cell death was induced only following dual stimulation (data not shown). The role of OX40/OX40L was underscored by the observation that antibody blockade of OX40L inhibited HIV-1 activation following OX40L stimulation. Antibody blockade also reversed HIV-1 reduction following dual stimulation with OX40L and TNF-α in ACH-2/OX40 and in M/IIIB-OX40 cells (Fig. 2B). Similarly, anti-OX40L blocking mAb partially or completely inhibited the cell deaths induced in ACH-2/OX40 and M/IIIB-OX40 cells following dual stimulation with OX40L and TNF-α (data not shown). The reduction of HIV-1 production resulting from dual receptor activation was also observed in the acutely HIV-1 NL4-3-infected Molt-4/CCR5-OX40 (M/R5-OX40) cells (Fig. 2C). This effect was also reversed by anti-OX40L blocking mAb. However, stimulation with OX40L alone did not enhance HIV-1 activation in acutely infected M/R5-OX40. The viability of the HIV-1 acutely infected M/R5-OX40 cells was rapidly reduced not only following dual stimulation with OX40L and TNF-α but also stimulation with OX40L alone as compared to ACH-2/OX40 and M/IIIB-OX40 cells (data not shown). This effect on cell viability was completely reversed with anti-OX40L blocking mAbs (data not shown). Therefore, these results support the view that OX40 stimulation by its natural ligand, OX40L, combined with stimulation by TNF-α, leads to a significant reduction of HIV-1 production, which is associated with rapid cell death, not only in an ACH-2 cell line, but also in Molt-4/IIIB, U1, and HIV-1 acutely infected Molt-4/CCR5 cell lines.

OX40 ligation-mediated cell death occurs independently of HIV-1

To determine whether the cell death of cells overexpressing OX40, induced by the stimulation with OX40L and/or TNF-α, was intrinsic to the cytopathic effects of HIV-1 infection, we established a series of HIV-1-negative/OX40-positive and control vector transfectants. These cells were stimulated by coculture with $OX40L^+$ cells in the presence or absence of TNF-α, followed by analysis of cell viability. As shown in Fig. 3A, cell death was seen in both the M/R5-OX40 and in the CEM/OX40 cells following stimulation by OX40L, and, furthermore, dual stimulation with OX40L and TNF-α synergistically accelerated the rate of cell death. In these two cell lines, TNF-α alone, at the doses utilized, had no effect on cell viability. On the other hand, in the case of another T cell line, Jurkat/OX40, and the two $CD4^+$ promonocytic cell lines, U937/OX40 and THP-1/OX40, dual receptor stimulation, but not OX40L stimulation alone, strongly induced cell death. However, the rate of cell death was more moderate in these cell lines than the rate observed with M/R5-OX40 and with CEM/OX40 cells. In contrast, the B cell line BJAB/OX40 was resistant to each of the stimulation protocols utilized above. As shown in Fig. 3B, death of OX40-expressing $CD4^+$ T cells, following stimulation with either OX40L or with OX40L and TNF-α, was completely inhibited by anti-OX40L blocking mAb. This shows that OX40 triggering by OX40L was necessary for the induction of cell death. Maximum cell death was observed under close cell-to-cell contact between $OX40^+$ responder and $OX40L^+$ stimulator cells and at higher TNF-α concentrations (more than 2 ng/ml) (Fig. 3C). Therefore, in the absence of HIV-1, OX40-mediated signaling is capable, on its own, of inducing cell death, and the dual stimulation with OX40L and TNF-α leads to an accelerated rate of cell death than stimulation with either ligand alone, which differs with respect to the cell line being studied.

OX40-mediated apoptosis in M/R5-OX40 cells is induced by signaling via the cytoplasmic tail of OX40 and by the caspase cascade

To confirm that the cell death, observed above, was dependent on signal transduction via OX40, we established a cell line expressing a deletion mutant of OX40 that lacked the cytoplasmic tail, Molt-4/CCR5-OX40del (M/R5-OX40del). M/R5-

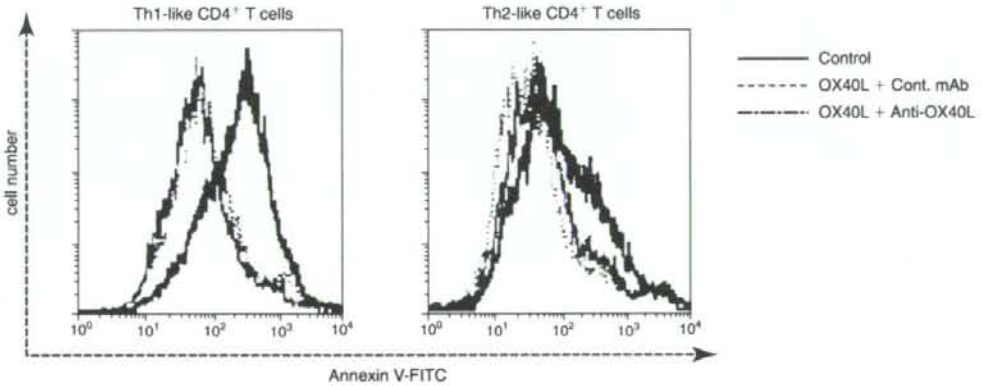

FIG. 6. Induction of apoptosis in primary activated $CD4^+$ T cells by cocultivation with OX40L-expressing cells. Two types of activated $CD4^+$ T cells from PBMCs of healthy donors, Th1-like and Th2-like, were activated in the presence of rhIL-12 and rhIL-4, respectively, on day 0, 3, and 6. After an additional 3 days, cells were cocultured with PFA-fixed SV-T2/OX40L (OX40L) or with PFA-fixed SV-T2/control (Control) cells in the presence of either anti-hOX40L blocking mAb (Anti-OX40L) or isotype control mAb (Cont. mAb). After 24 h, cells were stained by anti-hCD4-Cy5 and then stained by annexin V-FITC. Cells were analyzed with a FACSCalibur. Representative results from three independent experiments are shown.

OX40, M/R5-OX40del, and M/R5-control cells were stimulated with OX40L and/or TNF-α, followed by the determination of cell viability using annexin V-FITC/PI staining. At 24 h following stimulation, apoptosis was apparent in M/R5-OX40 cells; however, no detectable apoptosis was observed in M/R5-OX40del cells (Fig. 4A), suggesting a signal from OX40 is indeed required for apoptosis. On the other hand, M/R5-OX40 cells pretreated with the broad-spectrum caspase inhibitor z-VAD-fmk and stimulated with OX40L, in the absence or presence of TNF-α, were prevented from undergoing apoptosis (Fig. 4B), suggesting that the apoptosis was caspase cascade dependent. In accordance with this, Western blot assays showed that in OX40L-stimulated M/R5-OX40 cells, the levels of pr-caspase-8 (57 kDa) and procaspase-3 (32 kDa) were markedly reduced, and cleaved caspase-8 (43 kDa) was increased after OX40L stimulation (Fig. 4C). Taken together, these results indicate that the OX40-mediated apoptosis of M/R5-OX40 cells is dependent on both signaling via the cytoplasmic tail of OX40 and on the caspase cascade.

OX40-induced apoptosis in M/R5-OX40 cells is mediated by endogenous TNF-α

To explore the mechanisms involved in OX40-mediated apoptosis, M/R5-OX40 cells were examined in more detail, since these cells undergo apoptosis by OX40L stimulation without exogenous TNF. First, we examined the effects of various mAbs on OX40L-triggered cell death. As shown in Fig. 5A, anti-hTNF-α blocking mAb, but none of anti-hTNF-β, anti-hTRAIL, and anti-hFasL blocking mAbs, inhibited the cell death, showing that TNF-α, but not TNF-β, TRAIL, and FasL, was involved in cell death after OX40L stimulation. Indeed, OX40L-stimulated M/R5-OX40 cells synthesized TNF-α, which was detected in cell lysates, but not in culture supernatants (Fig. 5B). The fact that TNF-α was not detected in culture supernatants suggests that endogenously synthesized TNF-α bound to its membrane receptors (TNF-RI and/or TNF-RII) on the surface of cells stimulated with OX40L. The production of endogenous TNF-α was completely inhibited by anti-OX40L neutralizing mAb, showing that this endogenous TNF-α production was mediated by the OX40L/OX40 interaction (Fig. 5C). These results suggest that endogenous TNF-α, induced by OX40 stimulation in the OX40$^+$ T cell line M/R5-OX40 mediates apoptosis. Furthermore, we also determined the induction of endogenous TNF-α in other OX40$^+$ cell lines. As shown in Fig. 5D, although endogenous TNF-α was induced in the T cell line CEM/OX40, it was not dependent on OX40L stimulation, unlike M/R5-OX40 cells. Interestingly, in another T cell line, Jurkat/OX40, endogenous TNF-α was not detected. On the other hand, two promonocytic cell lines, U937/OX40 and THP-1/OX40, strongly expressed endogenous TNF-α regardless of OX40 stimulation. The B cell line BJAB/OX40 also weakly expressed endogenous TNF-α regardless of OX40 stimulation. In all of these cell lines, soluble TNF-α was not detected in the culture supernatants after OX40L stimulation (data not shown).

Apoptosis of primary CD4$^+$ T cells by cocultivation with OX40L-expressing cells

Finally, we determined whether apoptosis can be induced in primary CD4$^+$ T cells by OX40-stimulation *in vitro*. We generated two types of activated CD4$^+$ T cells from PBMCs of healthy donors, Th1-like and Th2-like, which were activated in the presence of IL-12 and IL-4, respectively. The Th1-like CD4$^+$ T cells expressed higher levels of functional OX40 than the Th2-like CD4$^+$ T cells.[45] These two types of cells were cocultured for 24 h with PFA-fixed SV-T2/OX40L or with PFA-fixed SV-T2/control cells in presence of either anti-hOX40L blocking mAb or isotype control mAb. As shown in Fig. 6, OX40 stimulation increased the levels of annexin V binding, especially in the Th1-like CD4$^+$ T cells. Since anti-OX40L mAb inhibited annexin V staining, these results suggest that under Th1-like conditions some fractions of primary CD4$^+$ T cells undergo apoptosis following OX40 stimulation.

DISCUSSION

We show here, for the first time, that combined OX40L and TNF stimulation leads OX40$^+$ T cell lines and primary CD4$^+$ T cells to undergo apoptosis. Apoptosis-inducing effects have been described for a number of HIV-1 proteins, including Env,[46] Tat,[47] Nef,[48] Vpr,[49] and Vpu.[50] Recently, Lenardo *et al.* have shown that HIV-1 can induce necrosis of CD4$^+$ T cells.[51] However, the data presented herein, using the OX40 transfectants of the HIV-1-negative T cell line Molt-4/CCR5, clearly demonstrate that OX40-mediated cell death is independent of apoptosis- or of necrosis-inducing effects of HIV-1 proteins.

Stimulation of other DD-lacking members of the TNF-R superfamily, including TNF-R2, CD27, CD30, and CD40, induces the death of tumor cells and of normal cells under certain conditions. One known mechanism for TNF-R2-, CD30-, and CD40-induced cell death is that receptor stimulation activates cells to produce endogenous membrane TNF, which stimulates the DD-containing TNF-R1 to induce cell death.[31] A second mechanism suggested for CD40-mediated cell death is an amplification of the Fas-dependent apoptosis pathway.[52] In this study, we show that apoptosis in M/R5-OX40 cells, induced by OX40 stimulation, was efficiently blocked by the caspase inhibitor z-VAD-fmk, and was also blocked by anti-TNF-α neutralizing mAb. Moreover, the apoptosis of OX40-stimulated M/R5-OX40 cells was associated with the induction of endogenous TNF-α. These results suggest that the OX40-mediated apoptosis in M/R5-OX40 cells occurs indirectly, via a TNF/TNF-R system reminiscent of that mediated via TNF-R2, CD30, and CD40.

The response to coactivation by OX40L plus TNF-α in Jurkat/OX40 cells is also of great interest. In Jurkat/OX40 cells, apoptosis was not induced by soluble TNF-α or by OX40 stimulation and endogenous TNF-α was not induced by OX40 stimulation, unlike the results observed in M/R5-OX40 cells. However, rapid apoptosis was induced in Jurkat/OX40 cells by costimulation with OX40L plus TNF-α. These results suggest a new aspect of OX40 function in the induction of apoptosis in this cell line upon costimulation with OX40L plus TNF-α. The degree to which this mechanism contributes to OX40-induced apoptosis in other cell lines, such as M/R5-OX40, CEM/OX40, U937/OX40, and THP-1/OX40, is not currently known. On the other hand, U937/OX40 and THP-1/OX40 cells were relatively resistant, and BJAB/OX40 cells were completely resistant to the combined stimulation with OX40L and TNF-α (Fig. 3A). Since endogenous TNF-α is expressed in these cells irrespec-

tive of stimulation, these cells might have an endogenous mechanism to resist TNF-α-induced apoptosis. Furthermore, since normal B cells and monocytic cells do not express OX40, it might be possible that they lack the machinery for OX40-mediated intracellular signaling, or are equipped with an, as yet, undetermined anti-OX40 signal. Further studies are required to define the mechanisms of such resistance. In addition, since apoptosis of CEM/OX40 cells following OX40L stimulation could not be completely inhibited by the caspase inhibitor z-VAD-fmk at concentrations up to 100 μM (data not shown), it is possible that OX40-induced cell death may include additional apoptotic pathways, which may depend upon the cell line being studied.

It can be speculated that the survival or the apoptotic fate of $CD4^+$ T cells, after OX40 stimulation, is dependent on immunological environments. Kawamata *et al.* have shown that the cytoplasmic tail of OX40 binds TRAF2 and TRAF5, leading to NF-κB activation.[12] TRAF2 is required for the TNF-mediated activation of c-Jun N-terminal kinase (JNK) and of NF-κB, which leads to the generation of antiapoptotic signals.[3] It has been shown that TRAF2 can trigger cell death in the presence of the receptor-interacting protein (RIP), whereas in the absence of RIP, TRAF2 activates NF-κB.[53] RIP has also been implicated in caspase-8-independent necrosis.[54] Furthermore, Li *et al.* have shown that activation of TNF-R2 induces ubiquitination and proteasomal degradation of TRAF2, leading to the enhancement of TNF-induced apoptosis.[55] In addition, it has been demonstrated that stimulation of TNF-R2, CD30, or CD40 leads to selective enhancement of TNF-R1-mediated caspase-8-dependent cell death by depletion of both TRAF2 and the antiapoptotic IAP proteins.[37] Another suggested mechanism for CD40L-mediated $CD4^+$ T cell death is failure of the induction of the antiapoptotic proteins Bcl-2 and Bcl-X_L.[56] However, this mechanism cannot explain OX40-mediated apoptosis, since OX40 activation has been shown to induce these two antiapoptotic proteins.[57] Recently, Ma *et al.* have shown that in both OX40 and 4-1BB-expressing cells, combined stimulation by OX40 and 4-1BB induces reduced NF-κB activation, cell survival, and cell growth.[58] At present, it remains unclear whether OX40 activation directly mediates cell death. Taken together, it is interesting to speculate that OX40 stimulation induces cell death via an apoptotic pathway mediated by its cytoplasmic tail. Further studies are in progress to reveal the precise molecular mechanisms of OX40-induced apoptosis of T cells in various immunological environments.

In conclusion, the present study revealed a novel immunological function of OX40 in OX40-expressing $CD4^+$ T cells, with the control of cell death, in the presence of TNF, potentially resulting in a reduction of HIV-1 production.

ACKNOWLEDGMENTS

This work was supported by grants from the Ministry of Education, Culture, Sports, Science and Technology of Japan, and the Ministry of Health, Labor and Welfare of Japan. We are grateful to Dr. A.A. Ansari (Emory University) for critical reading of this manuscript, Dr. H. Niwa (RIKEN) for the gift of the pCAGIPuro vector, and Dr. M. Baba (Kagoshima University) for the gift of the Molt-4/CCR5 cell line.

REFERENCES

1. Latza U, Durkop H, Schnittger S, *et al.*: The human OX40 homolog: cDNA structure, expression and chromosomal assignment of the ACT35 antigen. Eur J Immunol 1994;24:677–683.
2. Mallett S, Fossum S, and Barclay AN: Characterization of the MRC OX40 antigen of activated CD4 positive T lymphocytes: A molecule related to nerve growth factor receptor. EMBO J 1990;9:1063–1068.
3. Baker SJ and Reddy EP: Modulation of life and death by the TNF receptor superfamily. Oncogene 1998;17:3261–3270.
4. Tanaka Y, Inoi T, Tozawa H, Yamamoto N, and Hinuma Y: A glycoprotein antigen detected with new monoclonal antibodies on the surface of human lymphocytes infected with human T-cell leukemia virus type-I (HTLV-I). Int J Cancer 1985;36:549–555.
5. Miura S, Ohtani K, Numata N, *et al.*: Molecular cloning and characterization of a novel glycoprotein, gp34, that is specifically induced by the human T-cell leukemia virus type I transactivator p40tax. Mol Cell Biol 1991;11:1313–1325.
6. Baum PR, Gayle RB 3rd, Ramsdell F, *et al.*: Molecular characterization of murine and human OX40/OX40 ligand systems: Identification of a human OX40 ligand as the HTLV-1-regulated protein gp34. EMBO J 1994;13:3992–4001.
7. Ohshima Y, Tanaka Y, Tozawa H, Takahashi Y, Maliszewski C, and Delespesse G: Expression and function of OX40 ligand on human dendritic cells. J Immunol 1997;159:3838–3848.
8. Stuber E, Neurath M, Calderhead D, Fell HP, and Strober W: Cross-linking of OX40 ligand, a member of the TNF/NGF cytokine family, induces proliferation and differentiation in murine splenic B cells. Immunity 1995;2:507–521.
9. Morimoto S, Kanno Y, Tanaka Y, *et al.*: CD134L engagement enhances human B cell Ig production: CD154/CD40, CD70/CD27, and CD134/CD134L interactions coordinately regulate T cell-dependent B cell responses. J Immunol 2000;164:4097–4104.
10. Imura A, Hori T, Imada K, *et al.*: The human OX40/gp34 system directly mediates adhesion of activated T cells to vascular endothelial cells. J Exp Med 1996;183:2185–2195.
11. Baba E, Takahashi Y, Lichtenfeld J, *et al.*: Functional CD4 T cells after intercellular molecular transfer of OX40 ligand. J Immunol 2001;167:875–883.
12. Kawamata S, Hori T, Imura A, Takaori-Kondo A, and Uchiyama T: Activation of OX40 signal transduction pathways leads to tumor necrosis factor receptor-associated factor (TRAF) 2- and TRAF5-mediated NF-kappa B activation. J Biol Chem 1998;273:5808–5814.
13. Flynn S, Toellner FM, Raykundalia C, Goodall M, and Lane P: CD4 T cell cytokine differentiation: The B cell activation molecule, OX40 ligand, instructs CD4 T cells to express interleukin 4 and upregulates expression of the chemokine receptor, Blr-1. J Exp Med 1998;188:297–304.
14. Ohshima Y, Yang LP, Uchiyama T, *et al.*: OX40 costimulation enhances interleukin-4 (IL-4) expression at priming and promotes the differentiation of naive human CD4(+) T cells into high IL-4-producing effectors. Blood 1998;92:3338–3345.
15. Akiba H, Miyahira Y, Atsuta M, *et al.*: Critical contribution of OX40 ligand to T helper cell type 2 differentiation in experimental leishmaniasis. J Exp Med 2000;191:375–380.
16. Tanaka H, Demeure CE, Rubio M, Delespesse G, and Sarfati M: Human monocyte-derived dendritic cells induce naive T cell differentiation into T helper cell type 2 (Th2) or Th1/Th2 effectors. Role of stimulator/responder ratio. J Exp Med 2000;192:405–412.
17. Gramaglia I, Jember A, Pippig SD, Weinberg AD, Killeen N, and Croft M: The OX40 costimulatory receptor determines the development of CD4 memory by regulating primary clonal expansion. J Immunol 2000;165:3043–3050.

18. De Smedt T, Smith J, Baum P, Fanslow W, Butz E, and Maliszewski C: OX40 costimulation enhances the development of T cell responses induced by dendritic cells in vivo. J Immunol 2002;168:661–670.
19. Bansal-Pakala P, Jember AJ, and Croft M: Signaling through OX40 (CD134) breaks peripheral T-cell tolerance. Nat Med 2001;7:907–912.
20. Valzasina B, Guiducci C, Dislich H, Killeen N, Weinberg AD, and Colombo MP: Triggering of OX40 (CD134) on CD4(+)CD25+ T cells blocks their inhibitory activity: A novel regulatory role for OX40 and its comparison with GITR. Blood 2005;105:2845–2851.
21. Imura A, Hori T, Imada K, *et al.*: OX40 expressed on fresh leukemic cells from adult T-cell leukemia patients mediates cell adhesion to vascular endothelial cells: Implication for the possible involvement of OX40 in leukemic cell infiltration. Blood 1997;89:2951–2958.
22. Brocker T, Gulbranson-Judge A, Flynn S, Riedinger M, Raykundalia C, and Lane P: CD4 T cell traffic control: In vivo evidence that ligation of OX40 on CD4 T cells by OX40-ligand expressed on dendritic cells leads to the accumulation of CD4 T cells in B follicles. Eur J Immunol 1999;29:1610–1616.
23. Aten J, Roos A, Claessen N, Schilder-Tol EJM, Ten Berge IJM, and Weening JJ: Strong and selective glomerular localization of CD134 ligand and TNF receptor-1 in proliferative lupus nephritis. J Am Soc Nephrol 2000;11:1426–1438.
24. Ndhlovu LC, Ishii N, Murata K, Sato T, and Sugamura K: Involvement of OX40 ligand signals in the T cell priming events during experimental autoimmune encephalomyelitis. J Immunol 2001;167:2991–2999.
25. Murata K, Nose M, Ndhlovu LC, Sato T, Sugamura K, and Ishii N: Constitutive OX40/OX40 ligand interaction induces autoimmune-like diseases. J Immunol 2002;169:4628–4636.
26. Jember AG-H, Zuberi R, Liu FT, and Croft M: Development of allergic inflammation in a murine model of asthma is dependent on the costimulatory receptor OX40. J Exp Med 2001;193:387–392.
27. Arestides RS, He H, Westlake RM, *et al.*: Costimulatory molecule OX40L is critical for both Th1 and Th2 responses in allergic inflammation. Eur J Immunol 2002;32:2874–2880.
28. Uchiyama T: Human T cell leukemia virus type I (HTLV-I) and human diseases. Annu Rev Immunol 1997;15:15–37.
29. Kopf M, Ruedl C, Schmitz N, *et al.*: OX40-deficient mice are defective in Th cell proliferation but are competent in generating B cell and CTL responses after virus infection. Immunity 1999;11:699–708.
30. Ekkens MJ, Liu Z, Liu Q, *et al.*: The role of OX40 ligand interactions in the development of the Th2 response to the gastrointestinal nematode parasite Heligmosomoides polygyrus. J Immunol 2003;170:384–393.
31. Grell M, Zimmermann G, Gottfried E, *et al.*: Induction of cell death by tumour necrosis factor (TNF) receptor 2, CD40 and CD30: A role for TNF-R1 activation by endogenous membrane-anchored TNF. EMBO J 1999;18:3034–3043.
32. Prasad KV, Ao Z, Yoon Y, *et al.*: CD27, a member of the tumor necrosis factor receptor family, induces apoptosis and binds to Siva, a proapoptotic protein. Proc Natl Acad Sci USA 1997;94:6346–6351.
33. Mir SS, Richter BW, and Duckett CS: Differential effects of CD30 activation in anaplastic large cell lymphoma and Hodgkin disease cells. Blood 2000;96:4307–4312.
34. Lee SY, Park CG, and Choi Y: T cell receptor-dependent cell death of T cell hybridomas mediated by the CD30 cytoplasmic domain in association with tumor necrosis factor receptor-associated factors. J Exp Med 1996;183:669–674.
35. Hess S and Engelmann H: A novel function of CD40: Induction of cell death in transformed cells. J Exp Med 1996;183:159–167.
36. Chan FK and Lenardo MJ: A crucial role for p80 TNF-R2 in amplifying p60 TNF-R1 apoptosis signals in T lymphocytes. Eur J Immunol 2000;30:652–660.
37. Fotin-Mleczek M, Henkler F, Samel D, *et al.*: Apoptotic crosstalk of TNF receptors: TNF-R2-induces depletion of TRAF2 and IAP proteins and accelerates TNF-R1-dependent activation of caspase-8. J Cell Sci 2002;115:2757–2770.
38. Takahashi Y, Tanaka Y, Yamashita A, Koyanagi Y, Nakamura M, and Yamamoto N: OX40 stimulation by gp34/OX40 ligand enhances productive human immunodeficiency virus type 1 infection. J Virol 2001;75:6748–6757.
39. Biswas P, Smith CA, Goletti D, Hardy EC, Jackson RW, and Fauci AS: Cross-linking of CD30 induces HIV expression in chronically infected T cells. Immunity 1995;2:587–596.
40. Tozawa H, Andoh S, Takayama Y, *et al.*: Species-dependent antigenicity of the 34-kDa glycoprotein found on the membrane of various primate lymphocytes transformed by human T-cell leukemia virus type-I (HTLV-I) and simian T-cell leukemia virus (STLV-I). Int J Cancer 1988;41:231–238.
41. Tanaka Y, Yoshida A, Tozawa H, Shida H, Nyunoya H, and Shimotohno K: Production of a recombinant human T-cell leukemia virus type-I trans-activator (tax1) antigen and its utilization for generation of monoclonal antibodies against various epitopes on the tax1 antigen. Int J Cancer 1991;48:623–630.
42. Baba M, Miyake H, Okamoto M, Iizawa Y, and Okonogi K: Establishment of a CCR5-expressing T-lymphoblastoid cell line highly susceptible to R5 HIV type 1. AIDS Res Hum Retroviruses 2000;16:935–941.
43. Adachi A, Gendelman HE, Koenig S, *et al.*: Production of acquired immunodeficiency syndrome-associated retrovirus in human and nonhuman cells transfected with an infectious molecular clone. J Virol 1986;59:284–291.
44. Tanaka R, Yoshida A, Murakami T, *et al.*: Unique monoclonal antibody recognizing the third extracellular loop of CXCR4 induces lymphocyte agglutination and enhances human immunodeficiency virus type 1-mediated syncytium formation and productive infection. J Virol 2001;75:11534–11543.
45. Kondo K, Okuma K, Tanaka R, *et al.*: Requirements for the functional expression of OX40 ligand on human activated $CD4^+$ and $CD8^+$ T cells. Hum Immunol 2007;68:563–571.
46. Ohagen A, Ghosh S, He J, *et al.*: Apoptosis induced by infection of primary brain cultures with diverse human immunodeficiency virus type 1 isolates: Evidence for a role of the envelope. J Virol 1999;73:897–906.
47. Bartz SR and Emerman M: Human immunodeficiency virus type 1 Tat induces apoptosis and increases sensitivity to apoptotic signals by up-regulating FLICE/caspase-8. J Virol 1999;73:1956–1963.
48. Xu X-N, Laffert B, Screaton GR, *et al.*: Induction of Fas ligand expression by HIV involves the interaction of Nef with the T cell receptor zeta chain. J Exp Med 1999;189:1489–1496.
49. Hrimech M, Yao XJ, Bachand F, Rougeau N, and Cohen EA: Human immunodeficiency virus type 1 (HIV-1) Vpr functions as an immediate-early protein during HIV-1 infection. J Virol 1999;73:4101–4109.
50. Casella CR, Rapaport EL, and Finkel TH: Vpu increases susceptibility of human immunodeficiency virus type 1-infected cells to fas killing. J Virol 1999;73:92–100.
51. Lenardo MJ, Angleman SB, Bounkeua V, *et al.*: Cytopathic killing of peripheral blood CD4 (+) T lymphocytes by human immunodeficiency virus type 1 appears necrotic rather than apoptotic and does not require env. J Virol 2002;76:5082–5093.
52. Afford SC, Ahmed-Choudhury J, Randhawa S, *et al.*: CD40 activation-induced, Fas-dependent apoptosis and NF-kappaB/AP-1 signaling in human intrahepatic biliary epithelial cells. FASEB J 2001;15:2345–2354.

53. Pimentel-Muinos FX and Seed B: Regulated commitment of TNF receptor signaling: A molecular switch for death or activation. Immunity 1999;11:783–793.
54. Holler N, Zaru R, Micheau O, *et al.*: Fas triggers an alternative, caspase-8-independent cell death pathway using the kinase RIP as effector molecule. Nat Immunol 2000;1:489–495.
55. Li X, Yang Y, and Ashwell JD: TNF-RII and c-IAP1 mediate ubiquitination and degradation of TRAF2. Nature 2002;416:345–347.
56. Blair PJ, Riley JL, Harlan DM, *et al.*: CD40 ligand (CD154) triggers a short-term CD4(+) T cell activation response that results in secretion of immunomodulatory cytokines and apoptosis. J Exp Med 2000;191:651–660.
57. Rogers PR, Son J, Gramaglia I, Killeen N, and Croft M: OX40 promotes Bcl-xL and Bcl-2 expression and is essential for long-term survival of CD4 T cells. Immunity 2001;15:445–455.
58. Ma BY, Mikolajczak SA, Danesh A, *et al.*: The expression and the regulatory role of OX40 and 4-1BB heterodimer in activated human T cells. Blood 2005;106:2002–2010.

Address reprint requests to:
Yuetsu Tanaka
Department of Immunology
Graduate School of Medicine
University of the Ryukyus
Uehara 207
Nishihara, Okinawa 903-0215, Japan

E-mail: yuetsu@s4.dion.ne.jp

JOURNAL OF VIROLOGY, Nov. 2008, p. 10998–11008 Vol. 82, No. 22
0022-538X/08/$08.00+0 doi:10.1128/JVI.01311-08

Mouse APOBEC3 Restricts Friend Leukemia Virus Infection and Pathogenesis In Vivo▽

Eri Takeda,[1] Sachiyo Tsuji-Kawahara,[1] Mayumi Sakamoto,[1] Marc-André Langlois,[2] Michael S. Neuberger,[2] Cristina Rada,[2] and Masaaki Miyazawa[1]*

Department of Immunology, Kinki University School of Medicine, 377-2 Ohno-Higashi, Osaka-Sayama, Osaka 589-8511, Japan,[1] and Medical Research Council, Laboratory of Molecular Biology, Hills Road, Cambridge CB2 2QH, United Kingdom[2]

Received 24 June 2008/Accepted 3 September 2008

Several members of the apolipoprotein B mRNA-editing enzyme catalytic polypeptide-like complex 3 (APOBEC3) family in primates act as potent inhibitors of retroviral replication. However, lentiviruses have evolved mechanisms to specifically evade host APOBEC3. Likewise, murine leukemia viruses (MuLV) exclude mouse APOBEC3 from the virions and cleave virion-incorporated APOBEC3. Although the betaretrovirus mouse mammary tumor virus has been shown to be susceptible to mouse APOBEC3, it is not known if APOBEC3 has a physiological role in restricting more widely distributed and long-coevolved mouse gammaretroviruses. The pathogenicity of Friend MuLV (F-MuLV) is influenced by several host genes: some directly restrict the cell entry or integration of the virus, while others influence the host immune responses. Among the latter, the *Rfv3* gene has been mapped to chromosome 15 in the vicinity of the *APOBEC3* locus. Here we have shown that polymorphisms at the mouse *APOBEC3* locus indeed influence F-MuLV replication and pathogenesis: the *APOBEC3* alleles of F-MuLV-resistant C57BL/6 and -susceptible BALB/c mice differ in their sequences and expression levels in the hematopoietic tissues and in their abilities to restrict F-MuLV replication both in vitro and in vivo. Furthermore, upon infection with the pathogenic Friend virus complex, (BALB/c × C57BL/6)F_1 mice displayed an exacerbated erythroid cell proliferation when the mice carried a targeted disruption of the C57BL/6-derived *APOBEC3* allele. These results indicate, for the first time, that mouse APOBEC3 is a physiologically functioning restriction factor to mouse gammaretroviruses.

The apolipoprotein B mRNA-editing enzyme catalytic polypeptide-like editing complex 3 (APOBEC3) proteins are cellular cytidine deaminases with potent antiretroviral activities (reviewed in reference 8). Thus, after the penetration of retroviral nucleocapsids into target cells of infection and the initiation of reverse transcription, APOBEC3 enzymes can induce the conversion of cytosine to uracil in the minus-sense single-strand viral DNA, leading to G-to-A hypermutations in the subsequent plus-strand viral DNA. The resultant detrimental levels of mutations in the proviral genome, along with a deamination-independent mechanism that works prior to the proviral integration (9), together exert efficient antiretroviral effects in infected target cells. However, retroviruses have evolved to evade their natural hosts' APOBEC3. Thus, human immunodeficiency virus (HIV) counters the action of human APOBEC3G (hAPOBEC3G) through its viral infectivity factor (Vif). The Vif protein expressed in virus-producing cells interacts with hAPOBEC3G to recruit ubiquitin ligase complex and thus mediates polyubiquitination of hAPOBEC3G and Vif, resulting in rapid degradation of hAPOBEC3G (11, 29, 49). Vif is also known to partially impair de novo synthesis of hAPOBEC3G (45). Therefore, hAPOBEC3G is neutralized by HIV Vif, as well as simian immunodeficiency virus (SIV) Vif from the chimpanzee, rhesus macaque, and sooty mangabey (28). However, the antiretroviral effects of human APOBEC3 (hAPOBEC3) proteins are not limited to Vif-deficient lentiviruses of the above-mentioned primate species but are readily exerted with other lentiviruses including SIV from the African green monkey, equine infectious anemia virus, and more distantly related retroviruses such as murine leukemia virus (MuLV), porcine endogenous retrovirus, and foamy viruses (12, 16, 21, 27). The hAPOBEC3G has also been shown to restrict retrotransposition of Alu elements (10), indicating a possible physiological role for APOBEC3 proteins in protecting cells from endogenous retroelements.

Similarly, mouse APOBEC3 (mAPOBEC3) restricts the replication of HIV type 1 (HIV-1) without being countered by Vif (28, 42), whereas mouse gammaretroviruses are relatively resistant to mAPOBEC3 (1, 4, 13). This resistance of mouse gammaretroviruses to the APOBEC3 protein of their natural host seems to be mediated through the exclusion of mAPOBEC3 from MuLV particles and cleavage of virion-incorporated mAPOBEC3 by the viral protease (1, 4, 13). Interestingly, however, mouse mammary tumor virus (MMTV), a betaretrovirus, is susceptible to mAPOBEC3 (39), and evidence has been shown that endogenous polytropic and modified polytropic retroviruses have been genetically modified through the action of mAPOBEC3 (19). Thus, increasing evidence indicates a possible physiological role for mAPOBEC3 in restricting the replication of gammaretroviruses, not just betaretroviruses, of cognate origin; however, direct demonstration of the protective effects exerted by mAPOBEC3 on pathogenic MuLV infection has been lacking (4).

Friend virus (FV) is the pathogenic retrovirus complex composed of replication-competent Friend MuLV (F-MuLV), a

* Corresponding author. Mailing address: Department of Immunology, Kinki University School of Medicine, 377-2 Ohno-Higashi, Osaka-Sayama, Osaka 589-8511, Japan. Phone and fax: 81-72-367-7600. E-mail: masaaki@med.kindai.ac.jp.

▽ Published ahead of print on 10 September 2008.

prototypic ecotropic gammaretrovirus, and defective spleen focus-forming virus (SFFV). When integrated into erythroid progenitor cells, the SFFV component induces rapid proliferation and differentiation of these target cells, causing increased hematocrit values (polycythemia) and massive splenomegaly within a few weeks after inoculation into a susceptible strain of mice (5, 32, 36). This increase in the number of erythroid progenitor cells leads to increasing copy numbers of F-MuLV and SFFV proviruses and ultimately causes the emergence of erythroleukemia through promoter insertion or silencing of a tumor suppressor gene (22). The pathogenicity of FV is, however, influenced by several host genes: some directly restrict the target cell entry or integration of F-MuLV and SFFV, and others interfere with the growth potentiation of SFFV-infected erythroid progenitor cells (5, 32, 36). Yet other host genes, however, influence the FV-induced pathogenesis more indirectly by affecting the host immune response to the viral antigens. These include the major histocompatibility complex class I and class II genes that regulate $CD8^+$ and $CD4^+$ T-cell recognition of viral epitopes (33, 34); a class Ib gene putatively influencing natural killer cell activities toward FV-infected cells (18, 35); and a non-major histocompatibility complex gene, *Rfv3*, that influences the duration of viremia (6, 17, 47) partly through its effects on the production of virus-neutralizing antibodies (Ab) (23). The *Rfv3* gene has been mapped to within a narrow segment of mouse chromosome 15, colocalizing with the *APOBEC3* locus (23, 36), indicating that the possible polymorphisms in the *APOBEC3* locus might constitute a physiological resistance factor to FV infection in mice. We demonstrate here that an allelic variant of mAPOBEC3 expressed in C57BL/6 mice does restrict F-MuLV replication as well as FV-induced pathogenesis in vivo.

MATERIALS AND METHODS

Mice and virus. C57BL/6, BALB/c, B10.A/SgSn, and (BALB/c × C57BL/6)F_1 ($CB6F_1$) mice were purchased from Japan SLC, Inc., Hamamatsu, Japan. A/WySnJ mice were purchased from the Jackson Laboratory, Bar Harbor, ME. The mAPOBEC3-deficient mice have been described previously (31). They were backcrossed to C57BL/6 mice at least seven times and mated with BALB/c mice. Both male and female mice, 6 to 10 weeks old, were used for virus inoculation. All animals were housed and bred in the experimental animal facilities at Kinki University School of Medicine under a specific-pathogen-free condition, and the experiments described here have been approved by Kinki University. Replication-competent helper virus of the FV complex, F-MuLV, was purified from the culture supernatant of *Mus dunni* cells persistently infected with an infectious molecular clone, FB29 (44), as described previously (33).

Vector constructions. Total RNA was extracted from tissues and cells by using TRIzol reagent (Invitrogen, Carlsbad, CA), and cDNA synthesis was performed by using a SuperScriptIII first-strand synthesis system (Invitrogen). The primers described below were purchased from GeneDesign, Inc., Osaka, or Operon Biotechnologies, Tokyo, Japan. The full-length mAPOBEC3 cDNA were amplified by PCR using the oligonucleotide primers 5′-GGGGTACCGCCGCCACC ATGGGACCATTCTGTCTGGGATGCAGCCATCGC-3′ and 5′-GGTCTAG ACATCGGGGGTCCAAGCTGTAGGTTTCC-3′, with primary cDNA samples prepared from the spleens of C57BL/6 and BALB/c mice. The hAPOBEC3G and hAPOBEC3F cDNA were amplified by PCR using the primers 5′-GGGGTACCG CCGCCACCATGAAGCCTCACTTCAGAAACACAGTGGAGCG-3′ (for both hAPOBEC3G and hAPOBEC3F) and 5′-GGACCGGTGTTTTCCTGATTCTGG AGAATGGCCCGC-3′ (for hAPOBEC3G) or 5′-GGACCGGTCTCGAGAATC TCCTGCAGCTTGCTGTCCAGG-3′ (for hAPOBEC3F), with templates prepared from peripheral blood mononuclear cells of a healthy individual. The above-described APOBEC3 cDNA were cloned into the SalI/EcoRI digest (for mAPOBEC3) or HindIII/KpnI digest (for hAPOBEC3) of the pFLAG-CMV2 vector (Sigma-Aldrich Corp., St. Louis, MO.). The control plasmid pFLAG-CMV2-GFP was constructed by amplifying the green fluorescent protein (GFP) gene from the pEGFP vector (Clontech Laboratories, Inc., Mountain View, CA) with the oligonucleotide primers 5′-GGAAGCTTATGGTGAGCAAGGGCGAGGAGC-3′ and 5′-TCAGTACTTGTACAGCTCGTCCATGCCG-3′ and inserting it into the HindIII/EcoRI digest of the pFLAG-CMV2 vector.

The catalytic site mutants were produced based on the mAPOBEC3 cDNA lacking the exon 5 cloned from C57BL/6 mice ($mA3^b\Delta5$) by a quick-change site-directed mutagenesis using the pFLAG-CMV2-$mA3^b\Delta5$ plasmid as the template. The following primers were used to introduce each mutation (underlined). Primers 5′-CAACATCCACGCTGCAATCTGCTTTTTATACTGGTTCCATG ACAAAGTACTGAAAGTGCTGTCTCCG-3′ and 5′-GTACTTTGTCATGG AACCAGTATAAAAAGCAGATTGCAGCGTGGATGTTGTCCTTGTTCT TAAAGACCCC-3′ were used for the generation of $mA3^b\Delta5^{E73A}$, and primers 5′-AAAGGCAAACAGCATGCAGCAATCCTCTTCCTTGATAAG-3′ and 5′-TCTTATCAAGGAAGAGGATTGCTGCATGCTGTTTGCC-3′ were used for the generation of $mA3^b\Delta5^{E257A}$. The double mutant $mA3^b\Delta5^{E73A,\ E257A}$ was generated on pFLAG-CMV2-$mA3^b\Delta5^{E257A}$ by using the oligonucleotide pairs used for the generation of $mA3^b\Delta5^{E73A}$. These mutants were verified by DNA sequencing. The plasmids expressing the chimera between $mA3^b\Delta5$ and the mAPOBEC3 lacking the exon 5 cloned from BALB/c mice ($mA3^d\Delta5$), pFLAG-CMV2-$mA3^d\Delta5$/$mA3^b\Delta5$ and the reciprocal, pFLAG-CMV2-$mA3^b\Delta5$/$mA3^d\Delta5$, were constructed by mutually exchanging the cytidine deaminase catalytic domain 2 (CDD2)-encoding fragments between the $mA3^b\Delta5$ and the $mA3^d\Delta5$ cDNA at the unique HindIII site.

The plasmid vectors used for the establishment of stably expressing cells, the pIRES-PURO-FLAG-mA3, pIRES-PURO-FLAG-hA3, pIRES-PURO-FLAG, and pIRES-PURO-FLAG-GFP plasmids, were constructed by inserting the SpeI-XbaI fragment from the pFLAG-CMV2-mA3, pFLAG-CMV2-hA3, pFLAG-CMV2, and pFLAG-CMV2-GFP plasmids, respectively, into the SpeI/NheI digest of the pIRES-PURO vector (Clontech Laboratories, Inc.). These constructs were verified by DNA sequencing.

Establishment of stably transfected cell lines. To determine the possible restricting effects of the mAPOBEC3 allelic variants in a focus formation assay that mimics physiological MuLV replication, we established BALB/3T3 cell lines that stably expressed different FLAG-tagged versions of mAPOBEC3, the short isoform of mAPOBEC3 derived from C57BL/6 mice ($mA3^b\Delta5$) and the full-length ($mA3^d$) and the short ($mA3^d\Delta5$) isoforms derived from BALB/c mice (Fig. 1). DNA transfection into BALB/3T3 cells was performed by using Lipofectamine 2000 reagent (Invitrogen). For the establishment of stable transfectants, cells expressing FLAG peptide (FLAG) and FLAG-fusion proteins (FLAG-proteins) were selected in the presence of 6 μg/ml puromycin (Sigma-Aldrich) and 200 μg/ml Geneticin (GIBCO Industries Inc., Los Angeles, CA), and colony-forming cells were picked into a well of 96-well culture plates. The expression of FLAG and FLAG-proteins was confirmed by immunoblotting analyses of the cell lysates and with immunofluorescence staining of the cells.

PCR analysis of mAPOBEC3 mRNA and genomic DNA. Endogenous mAPOBEC3 and GAPDH mRNA from tissues and cells were detected by reverse transcription-PCR (RT-PCR) using primers 5′-GGGGTACCGCCGCCAC CATGGGACCATTCTGTCTGGGATGCAGCCATCGC-3′ and 5′-GGTCTA GACATCGGGGGTCCAAGCTGTAGGTTTCC-3′ for the full-length mAPOBEC3; primers 5′-TTACAAATTTTAGATACCAGGATTCTAAGCTTCAGG AG-3′ and 5′-TTGGTTGTAAAACTGCGAGTAAAATTCCTCTTCAC-3′ for the mAPOBEC3 exon 5 region; and primers 5′-GCCAAGGCTATCCATGAC AACTTTGG-3′ and 5′-GCCTGCTTCACCACCTTCTTGATGTC-3′ for mouse GAPDH. Genomic allele analyses of APOBEC3-deficient mice were done by detecting the insertion of a neomycin resistance gene in the exon 3 (31) by using the oligonucleotide primers 5′-CCCCCCAAGGACAACATCCACGCTG-3′ and 5′-GGCGGCAGGCGATTCAGGCCTTGGAA-3′.

Quantitative real-time PCR analyses of mAPOBEC3 mRNA. Real-time PCR assays for quantitative comparisons of mAPOBEC3 mRNA expression levels were performed as described previously (36). The mAPOBEC3 fragment was amplified from 50 ng of total cDNA and quantified using Platinum Quantitative PCR SuperMix-UDG with 6-carboxyl-X-rhodamine (ROX) reference dye (Invitrogen) with an Applied Biosystems 7900HT Fast Real-Time PCR system (Applied Biosystems, Foster City, CA). The primers and 6-carboxyfluorescein (FAM) dye-labeled probe used for the quantification of mAPOBEC3 messages were as follows. Primers were 5′-GCGGCTCCACAGGATCAA-3′ and 5′-TCC AAGCTGTAGGTTTCCAAAGT-3′; and the probe was 5′-TCTGCAAGATT GGTGAAT-3′. After initial incubations at 50°C for 2 min and 95°C for 10 min, 40 cycles of amplification were carried out for 15 s at 95°C, followed by 1 min at 60°C. TaqMan rodent GAPDH control reagent (Applied Biosystems) was used as an internal control.

Northern and Western blot analyses. Total RNA was prepared from mouse tissues by using TRIzol reagent. Two micrograms of the RNA was denatured

FIG. 1. Alleles and isoforms of mAPOBEC3 in FV-resistant C57BL/6 and -susceptible BALB/c mice. (A) The known genomic organization and splicing pattern of the mouse *APOBEC3* gene is shown with short arrows indicating the positions of the PCR primers used. (B) Alignment of the amino acid sequences of mAPOBEC3 for the C57BL/6-derived exon 5-lacking isoform (mA3$^{b}\Delta5$) (GenBank accession no. NM_030255), and BALB/c-derived full-length (mA3^{d}) [BC003314] and exon 5-lacking (mA3$^{d}\Delta5$) isoforms (GenBank accession no. EDL04624). Open boxes show different amino acid residues, shaded boxes show the regions necessary for CDD activities, and the long horizontal lines indicate two CDDs as described in previous reports (15, 37). B10.A/SgSn mice showed amAPOBEC3 sequence that was completely identical to that of C57BL/6 mice, while A/WySn mice shared the mAPOBEC3 sequence with BALB/c mice.

with RNA loading mixture (GenHunter Corporation, Nashville, TN), separated in a 1% formaldehyde-agarose gel, transferred to nitrocellulose membrane, and hybridized with ^{32}P-labeled probes that were prepared by random priming with the templates generated by RT-PCR (mAPOBEC3, 5′-CCCGTCTCCCTTCAC CATGGGG-3′ and 5′-GGGAGACCTTTTGTTAGACAGATATTTGACAGA GTGG-3′; and mouse β-actin, 5′-ATGGATGACGATATCGCTGCGCTGGT CGTCGACAACGGCTCCGGC-3′ and 5′-GGTCATCTTTTCACGGTTGGC CTTAGGGTTCAGGGGGGCC-3′). Specific hybridization was visualized using a BAS-MS imaging plate (Fujifilm Corp., Tokyo, Japan). Densitometric analyses of the detected bands were done by using Image Gauge software (Fujifilm Corp.), and the results were normalized with GAPDH for each sample. Anti-FLAG M2 (Sigma-Aldrich) and anti-actin (Santa Cruz Biotechnology Inc., Santa Cruz, CA) Ab were purchased from the above-mentioned suppliers. Horseradish peroxidase-conjugated secondary Ab was purchased from Zymed Laboratories (San Francisco, CA). Detection by immunoblotting of F-MuLV gp70 and p30^{gag} with monoclonal antibodies (MAb) 720 and R18-7 has been described previously (40).

F-MuLV infection in vitro and APOBEC3 packaging analysis. BALB/3T3 cells stably expressing FLAG-APOBEC3 were seeded at 3×10^4 cells/well in 24-well plates and infected with purified F-MuLV at a multiplicity of infection of 2.0 in the presence of 1 μg/ml Polybrene (Sigma-Aldrich). After 2 h of incubation, the cells were washed, fed with fresh medium, and cultured for 2 days. For packaging analyses, the culture supernatants were centrifuged to remove cells, and viral particles were precipitated with polyethylene glycol and step purified into a 15%/85% sucrose interface (33). For flow cytometry analyses of the surface gp70 expression, F-MuLV-infected transfectants were detached from culture wells with a brief trypsin treatment and stained with biotinylated MAb 720 (40), followed by an incubation with allophycocyanin-conjugated streptavidin (eBioscience Inc., San Diego, CA), and were analyzed with a Becton-Dickinson (Franklin Lakes, NJ) FACScalibur system.

Sequence analysis of proviral DNA. F-MuLV in 1 ml of culture medium were inoculated onto a culture of *Mus dunni* cells and incubated for 18 h. After trypsinization and washing, the cells were treated with RNase I, and their DNA was isolated by using DNeasy (Qiagen, Hilden, Germany). A 1.2-kbp fragment of the F-MuLV proviral genome harboring the U3 and a part of the *gag* sequence was amplified by PCR using the primers 5′-CGGGATCCAAGGACCTGAAA TGACCCTG-3′ and 5′-GAAGAGAGAGGGGAGGTTTAGGG-3′. The amplified fragments were cloned into the pCR-Blunt vector using a Zero Blunt TOPO PCR cloning kit (Invitrogen). Sequencing was performed by using the T7 and T3 primers.

PCR quantification of F-MuLV genomic RNA and integrated proviral DNA. F-MuLV viral RNA in culture medium was purified with a QIAamp viral RNA kit (Qiagen) and cDNA generated by RT with SuperScriptIII First-Strand synthesis system (Invitrogen) after a treatment with DNase I (Invitrogen). Genomic DNA was purified from F-MuLV-infected BALB/3T3 cells expressing FLAG or FLAG-protein or *Mus dunni* cells infected with F-MuLV as described above. Viral DNA was quantified using Platinum Quantitative PCR SuperMix-UDG with ROX and a 7900HT Fast Real-Time PCR system. Primers for the detection of the F-MuLV genome and the FAM-labeled probe were designed for the *env* region by using the following oligonucleotides. Primers were 5′-AAGTCTCCC

CCCGCC-3′ and 5′-AGTGCCTGGTAAGCTCCCTGT-3′; and the FAM-labeled probe was 5′-ACTCCACATTGATTTCCCCGTCC-3′. After initial incubations at 50°C for 2 min and 95°C for 10 min, 40 cycles of amplification were carried out for 30 s at 95°C, followed by 1 min at 60°C. TaqMan rodent GAPDH control reagent was used as an internal control for genomic DNA.

Quantification of F-MuLV gp70 in culture supernatant. Ninety-six-well plates were coated with the gp70-specific MAb 48 (7) at 0.5 mg/well in 0.1 M $NaHCO_3$. Wells were blocked with 10% fetal bovine serum and incubated with a culture supernatant containing F-MuLV for 2 h at room temperature. After washing with PBS containing 0.05% Tween 20, 2 μg/well biotin-conjugated MAb 720 (40) was added and incubated for 1 h. After washing, the plates were incubated with a 1:30,000 dilution of horseradish peroxidase-conjugated streptavidin (Zymed Laboratories), and the chromogenic reaction was performed with 3,3′,5,5′-tetramethylbenzidine (Wako Pure Chemical Industries, Ltd., Osaka, Japan). The assay signals were measured as optical density at 450 nm, and the gp70 concentration was determined by adjusting it to the standard curve set with purified F-MuLV particles.

F-MuLV infection in vivo. C57BL/6 mice were inoculated with 1×10^5 focus-forming units (FFU) of F-MuLV by injecting 0.5 ml of a dilution via the tail vein. The spleen and bone marrow were removed, and single-cell suspensions were prepared for infectious center assays. $CB6F_1$ mice were inoculated with 1×10^4 FFU of F-MuLV.

F-MuLV infectivity and infectious center assays. These assays were performed as described previously (24, 46). In brief, 1 ml of culture supernatant from F-MuLV-infected FLAG- or FLAG-protein-expressing BALB/3T3 cells was diluted serially and plated in duplicate with 1 μg/ml Polybrene on monolayers of *Mus dunni* cells. For infectious center assays, spleen or bone marrow cell suspensions were serially diluted and plated at concentrations between 1.0×10^3 and 1.0×10^6 cells/well onto monolayers of *Mus dunni* cells. After being washed and fixed with methanol on the second day of coculturing, F-MuLV-infected cell foci were visualized with MAb 720 as described previously (40).

FV complex and assessment of its pathogenicity in vivo. A B-tropic FV complex free of lactate dehydrogenase-elevating virus was kindly provided by K. J. Hasenkrug, Laboratory of Persistent Viral Diseases, NIH, NIAID, Rocky Mountain Laboratories, Hamilton, MT. Inoculation of $CB6F_1$ mice with FV complex, monitoring of hematocrit values, and flow cytometry analyses of bone marrow cells were performed as described previously (18, 24).

Statistics. One-way analysis of variance (ANOVA) for the comparison of multiple groups was performed using GraphPad Prism software, version 5.0 (GraphPad Software, Inc., San Diego, CA), with an indicated posttest. When significant differences were pointed out by the ANOVA analyses, an individual level of significance was calculated for each pair of groups by two-tailed Student's or Welch's *t* test, depending on whether the variances were regarded as equal or not, respectively. Frequencies of mutations were evaluated by two-sided Fisher's exact test, between selected groups following an extended Fisher's exact test performed for the entire contingency table.

RESULTS

Allelic differences at the *APOBEC3* locus between FV-resistant and -susceptible strains of mice. The *Rfv3* gene that influences the duration of viremia after FV infection has been mapped to a segment of mouse chromosome 15 harboring the *APOBEC3* gene (17, 23, 36, 47); this led us to explore possible allelic differences in the expression of mAPOBEC3. We found that mAPOBEC3 mRNA expression levels in the hematopoietic tissues from naturally FV-resistant C57BL/6 and B10.A/SgSn mice were higher than those in susceptible BALB/c and A/WySnJ mice (Fig. 2A). Quantitative real-time PCR analyses confirmed that C57BL/6 and B10.A/SgSn mice expressed three- to fourfold higher levels of mAPOBEC3 mRNA than BALB/c and A/WySn mice did, both in the spleen and bone marrow (Fig. 2B). In addition, the mAPOBEC3 isoforms derived from C57BL/6 and BALB/c mice differed at several amino acid residues, five of which were located within the CDD1 (Fig. 1). Interestingly, A/WySnJ mice lacking the ability to control viremia (6) and to produce F-MuLV-neutralizing Ab (23) shared the mAPOBEC3 sequence with BALB/c mice.

Additional variability between mouse strains was also observed in part for the relative amounts of the two splice isoforms of mAPOBEC3. The mAPOBEC3 cDNA obtained by RT-PCR amplification from C57BL/6 mice was slightly smaller than that from BALB/c mice (Fig. 2C), and this was due to the lack of a 99-bp stretch corresponding to the exon 5 (Fig. 1). The use of primers placed in exons 4 and 6 showed that the predominant mAPOBEC3 mRNA isoform expressed in C57BL/6 mice lacked exon 5, while BALB/c mice expressed full-length mAPOBEC3 with very low levels of the short isoform (Fig. 2C). $CB6F_1$ mice expressed readily detectable full-length and truncated isoforms, with the latter in excess. Although the observed differences in the intensities of the PCR product bands might reflect different efficiencies in the amplification of the short and long fragments, the observed high intensity of the short-fragment band in C57BL/6 mice and the low intensity of the long-fragment band in BALB/c mice (Fig. 2C) are in agreement with the results of the Northern blotting (Fig. 2A) and real-time PCR (Fig. 2B) analyses. Thus, it is reasonable to conclude that BALB/c mice express a low level of full-length messages and C57BL/6 mice a high level of truncated mAPOBEC3 messages.

In vitro restriction of F-MuLV replication with C57BL/6-derived mAPOBEC3. It has been shown that mAPOBEC3 lacking the exon 5 (mAPOBEC3Δ5) can be packaged into MuLV particles more efficiently than the full-length mAPOBEC3 protein and, thus, can exert partial restriction of MuLV integration (1), although a recent report (4) has indicated similarly efficient incorporation of the full-length and the exon 5-lacking mAPOBEC3 into MuLV virions. However, the previous reports of the possible restricting effects of mAPOBEC3 on MuLV integration employed acute transfection of mAPOBEC3-expressing vector into MuLV packaging cells and examined a single-round integration of the MuLV vector and resultant expression of an inserted indicator gene. We intended to examine the possible restricting effects of mAPOBEC3 isoforms on more physiological replication cycles of infectious MuLV. Thus, we established BALB/3T3 cell lines that stably expressed different FLAG-tagged versions of mAPOBEC3 and measured the infectivity of F-MuLV produced from the transfectants in a focus formation assay that mimics physiological MuLV replication. BALB/3T3 cells stably expressing hAPOBEC3G, hAPOBEC3F, or GFP were also established as controls. These transfectants expressed comparable levels of APOBEC3 mRNA and produced APOBEC3 proteins of the expected sizes (Fig. 2D and F). Acute infection of the BALB/3T3 lines with an infectious molecular clone of F-MuLV resulted in a similar range of the envelope glycoprotein gp70 detected in the lysates, regardless of the APOBEC proteins expressed (Fig. 2F). The levels of F-MuLV infectivity and gp70 expression in the transfected lines were also confirmed to be similar by flow cytometric analyses (Fig. 2E). However, when we measured the infectivities of progeny viruses produced from the stable transfectants by focus formation assays on fully permissive *Mus dunni* cells, we found wide differences depending on the particular APOBEC3 protein expressed (Fig. 2H). Thus, the infectivity of F-MuLV produced from the $mA3^b\Delta5$-expressing cells was drastically reduced to a level similar to that obtained with F-MuLV derived from the hAPOBEC3G-expressing cells, whereas some 2.0×10^4 FFU/ml of infectious particles were

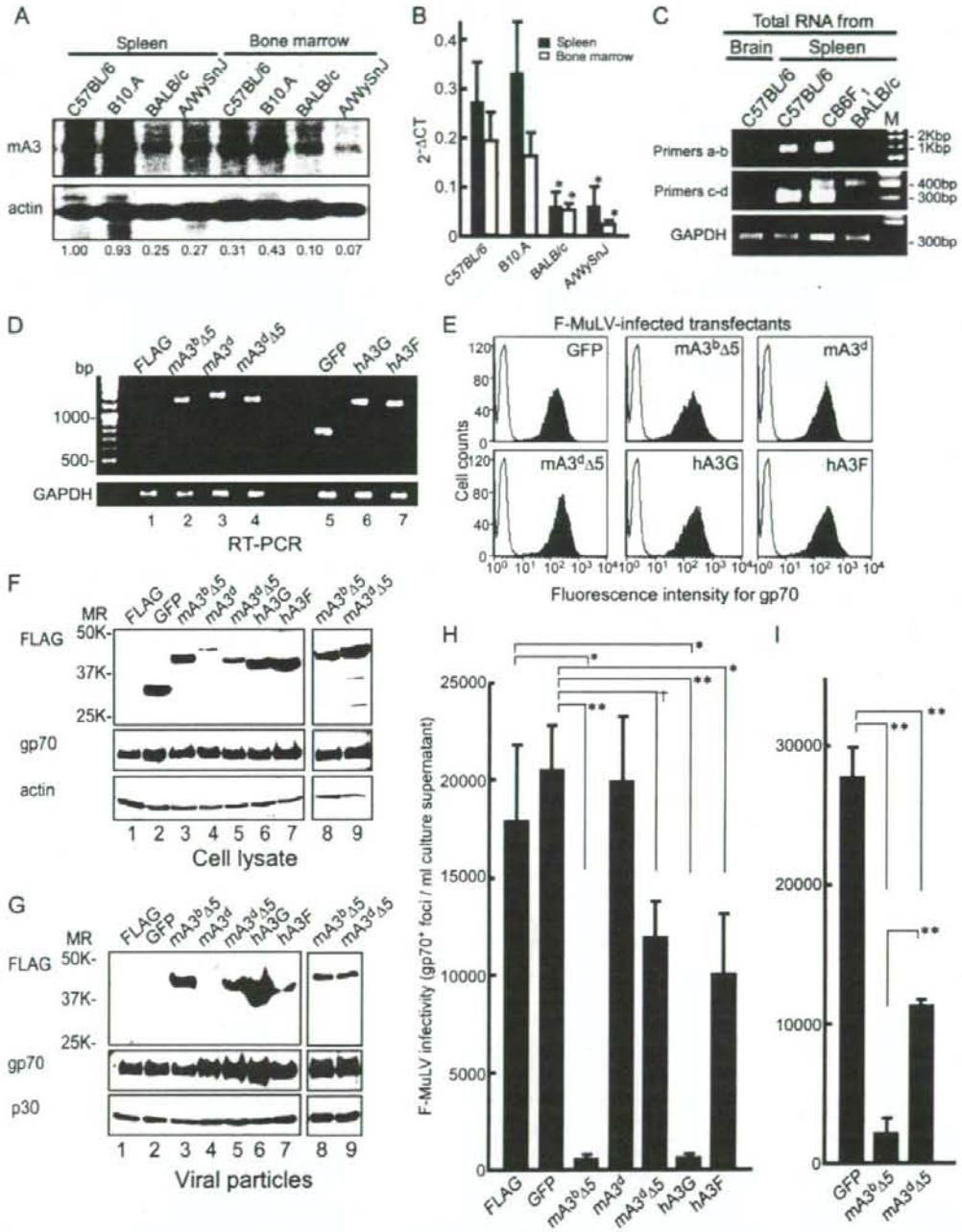

FIG. 2. Expression of the different alleles and isoforms of mAPOBEC3 in FV-resistant and -susceptible mice and infectivities of F-MuLV virions produced from mAPOBEC3-expressing cells. (A) Comparisons of mAPOBEC3 mRNA expression levels between mouse strains, by Northern blotting. Female mice, 7 to 8 weeks old, were analyzed for endogenous mAPOBEC3 mRNA expression. mAPOBEC3 mRNA was detected in 5 μg total RNA extracted from the spleen and bone marrow of the indicated strains of mice. β-Actin was used as an internal control. The numbers shown below each lane indicate densitometric ratios of expression levels between mAPOBEC3 and β-actin messages, normalized to that in the spleen of C57BL/6 mice. (B) Levels of expression of mAPOBEC3 mRNA relative to GAPDH quantified by real-time PCR are shown. Means of three samples each are shown with bars indicating standard errors of the means. *, statistically significant differences from the expression

TABLE 1. Number of F-MuLV provirus, infectious particles, and provirus in cells infected with progeny virus

Stable transfectant	Proviral copy no. (mean ± SEM) in producer cells (10^4)[a]	Concn (μg/ml) of gp70 (mean ± SEM) in culture supernatant[b]	Viral genomic copy no. (mean ± SEM) in culture supernatant (10^6)[c]	Proviral copy no. (mean ± SEM) in indicator cells (10^4)[e]
FLAG	99.47 ± 21.23	87.61 ± 4.76	5.43 ± 0.47	14.38 ± 4.79
GFP	156.80 ± 31.84	70.97 ± 11.17	4.06 ± 0.29	18.89 ± 4.00
mA3^{b}Δ5	140.19 ± 23.25	73.01 ± 7.63	3.17 ± 0.40	0.57 ± 0.05[f]
mA3^d	94.57 ± 24.01	70.71 ± 15.41	5.05 ± 0.71	16.45 ± 1.74
mA3^{d}Δ5	128.18 ± 23.60	72.57 ± 13.27	4.18 ± 0.31	4.59 ± 1.25[f]
hAPOBEC3G	53.78 ± 4.43	53.35 ± 8.44	2.82 ± 0.33[d]	0.35 ± 0.05[f]
hAPOBEC3F	99.80 ± 2.99	65.95 ± 6.05	3.54 ± 0.78	2.55 ± 0.40

[a] F-MuLV proviral DNA was quantified in the genomic DNA of the infected cells by quantitative real-time PCR using an F-MuLV-specific probe and primers. Data shown are means ± standard errors of the means (SEM) of copies per 50 ng of cellular genomic DNA, calculated from three repeated experiments. One-way ANOVA with Tukey's posttest for multiple comparisons indicated a significant difference only between GFP and hAPOBEC3G, but this was not significant ($P = 0.08$) by individual analysis using Welch's t test.

[b] Concentration of F-MuLV structural protein gp70 in culture supernatant from the acutely infected stable transfectants was analyzed by captured enzyme-linked immunosorbent assay using anti-gp70 MAb. Data shown here are means ± SEM calculated from three repeated experiments. No significant differences between the groups were found by one-way ANOVA with Tukey's posttest.

[c] Viral genomic RNA in the culture supernatant from the acutely infected stable transfectants was quantified by quantitative RT-PCR. Data shown here are means ± SEM of copies per 1 ml culture supernatant calculated from 3 repeated experiments. One-way ANOVA with Tukey's posttest indicated a significant group-wise difference only between the FLAG and hA3G.

[d] Student's t test for individual level of significance gave a P value of 0.011.

[e] F-MuLV proviral DNA was quantified from infected *Mus dunni* cells as described in the text. One-way ANOVA with Tukey's posttest for multiple comparisons indicated significant group-wise differences, which were then individually analyzed by t test.

[f] $P < 0.05$, in comparison with that of GFP.

detected when the supernatants from the BALB/3T3 cells expressing FLAG alone or control GFP were tested (Fig. 2H). In contrast, only a marginal reduction in F-MuLV infectivity was observed for the supernatant of mA3^{d}Δ5-expressing cells. Enforcing higher levels of expression of the mA3^d cDNA in the BALB/3T3 cells, compared with a low expression level of the endogenous *mA3^d* allele (Fig. 2D, lanes 1 and 3), did not result in any significant decrease in the infectivity of the virus produced (Fig. 2H), although the detectable amounts of mA3^d protein were apparently lower than those of the exon 5-lacking isoforms in several tested clones, which might have caused inefficient incorporation of the full-length protein into the virions (Fig. 2G). Nevertheless, these results indicate strain-dependent differences in F-MuLV-restricting activities of mAPOBEC3, with the C57BL/6-derived short isoform restricting F-MuLV with an efficacy similar to that shown by heterologous hAPOBEC3G.

When F-MuLV particles were purified from the culture supernatant of acutely infected transfectants, virion-incorporated mAPOBEC3 lacking the exon 5, but not the full-length mAPOBEC3, was readily detectable along with viral gp70 and p30^{gag}, regardless of their strains of origin (Fig. 2G). Interestingly, although mA3^{d}Δ5 derived from BALB/c mice was incorporated into F-MuLV as efficiently as C57BL/6-derived mA3^{b}Δ5 (Fig. 2G), only mA3^{b}Δ5 inhibited F-MuLV replication as strongly as hAPOBEC3G did in vitro (Fig. 2H). To exclude the possibility that the difference observed for the effects of mA3^{b}Δ5 and mA3^{d}Δ5 in restricting F-MuLV replication in vitro was caused by the slightly smaller amount of mA3^{d}Δ5 than mA3^{b}Δ5 detected in the transfectants used (Fig. 2F), we examined separate pairs of the stable transfectants. As shown in lanes 8 and 9 in Fig. 2 F and G, a higher level of mA3^{d}Δ5 was detected in the separate clone of stable transfectant, and the detected levels of virion-incorporated mAPOBEC3Δ5 proteins were similar. Nevertheless, the progeny virus produced from the mA3^{d}Δ5-expressing cells showed only about 60% reduc-

levels in B10.A/SgSn mice, indicated by one-way ANOVA with Dunnett's posttest for multiple comparisons ($P < 0.05$). (C) Splicing variants of the *APOBEC3* gene expressed in C57BL/6 and BALB/c mice. The known genomic organization and splicing pattern of the *APOBEC3* gene along with the positions of the primers used are shown in Fig. 1. The primers a and b amplified the entire mAPOBEC3-coding region, while primers c and d encompassed exons 4 and 6. GAPDH was used as an internal control. (D) Expression of APOBEC3 mRNA in the BALB/3T3 cells stably transfected with each *APOBEC3* gene was analyzed by RT-PCR. The same primers for mAPOBEC3 were used for samples in lanes 1 to 4. Samples in lanes 5 to 8 were amplified with each specific primer set. GAPDH was used as an internal control. Note the faint band of endogenous mA3^d cDNA in lane 1. (E) Flow cytometric analyses of the cell surface expression of F-MuLV gp70 on acutely infected stable transfectants are shown. Cells expressing the indicated genes were infected with F-MuLV at a multiplicity of infection of 2.0 and analyzed for surface gp70 expression with MAb 720 2 days later. (F and G) Proteins detected in cell lysate (F) and virus particles in the culture supernatant (G) from the infected BALB/3T3 cells expressing FLAG and FLAG-proteins are shown. Immunoblot detection was performed with the anti-FLAG, anti-gp70, anti-p30 or anti-actin Ab. (H and I) Infectivities of progeny F-MuLV produced from APOBEC3-expressing BALB/3T3 cells. *Mus dunni* cells were infected with the progeny virus produced from the indicated transfectants, and foci of infected cells were stained with anti-gp70 MAb for enumeration. The vertical axis in panel I shows F-MuLV infectivity as in panel H. The infectivities are shown as an equivalent of infectious virus per 1 ml of culture supernatant ($n = 3$, mean ± standard deviation; *, $P < 0.05$; †, $P < 0.01$; **, $P < 0.005$). The F-MuLV infectivity detected in the supernatant of hAPOBEC3G-expressing cells was drastically reduced, while only a moderate reduction in F-MuLV infectivity was observed when the indicator cells were inoculated with the supernatant from the hAPOBEC3F-expressing cells, consistent with the previous reports (1, 4, 13). All the experiments shown in panels C to I were performed with at least two representative clones of stable transfectants for each gene, and the results obtained with the independent clones were in agreement with the data shown.

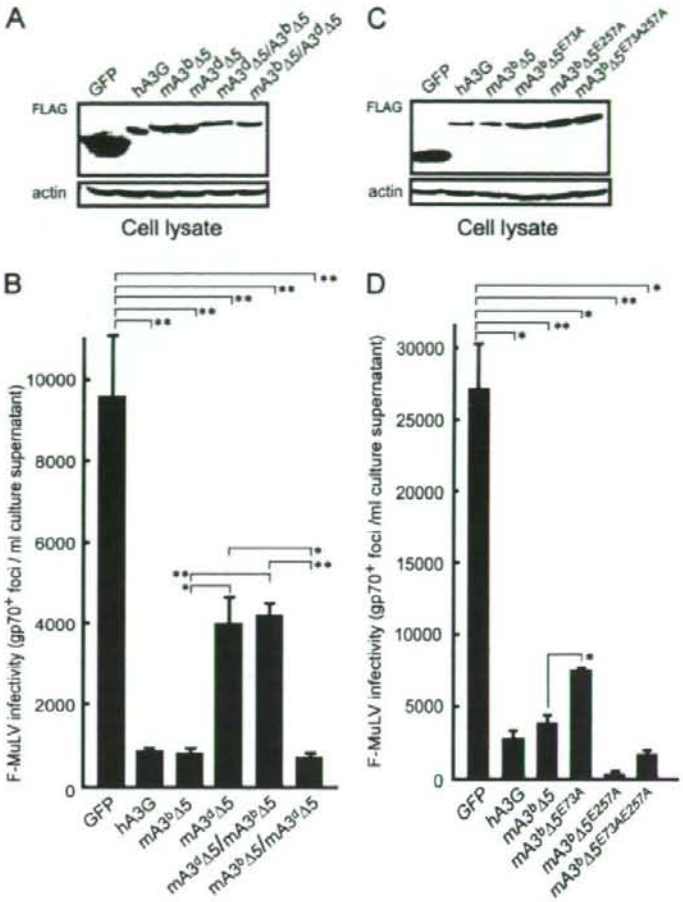

FIG. 3. Infectivities of F-MuLV virions produced from BALB/3T3 cells expressing mA3^{b}Δ5 mutants. (A and C) Cell lysates from the acutely infected transfectants were analyzed for the presence of APOBEC3 proteins. Immunoblot detection was performed with anti-FLAG and anti-actin Ab. (B and D) *Mus dunni* cells were infected with virus produced from the mAPOBEC3Δ5-expressing BALB/3T3 cells, and foci of gp70$^+$-infected cells were enumerated ($n = 3$, mean ± standard deviation; *, $P < 0.05$; **, $P < 0.005$). All the experiments shown were performed with at least two representative clones of stable transfectants for each gene, and the results obtained with the independent clones were in agreement with the data shown here.

tion in F-MuLV infectivity, while the progeny virus produced from the mA3^{b}Δ5-expressing cells showed vastly reduced infectivity, which was significantly lower than that shown by the mA3^{d}Δ5-containing F-MuLV.

The effectiveness of virion-incorporated mAPOBEC3 in restricting F-MuLV replication was further confirmed by quantitative analyses of viral copy numbers. Whereas neither the numbers of F-MuLV proviruses within the acutely infected stable transfectants nor the amounts of viral gp70 and genomic RNA in the supernatants were significantly different, regardless of the APOBEC3 or control genes expressed by the transfectants (Table 1), with the exception of a slight reduction in viral RNA in supernatants from the hAPOBEC3G-expressing cells, the number of F-MuLV proviral copies detected in infected *Mus dunni* indicator cells was reduced to less than 1/20 of the number detected in the cells infected with the control preparations when progeny virions were produced from mA3^{b}Δ5- or hAPOBEC3G-expressing cells. The number of proviral copies in the indicator cells was only moderately reduced when infected with progeny viruses produced from the mA3^{d}Δ5-expressing cells, and no reduction in the proviral copy numbers was observed for the cells infected with the virus produced from cells expressing the full-length mA3^d (Table 1). Thus, in agreement with the results of the infectious focus formation assays (Fig. 2H and I), mA3^{b}Δ5 restricts F-MuLV proviral integration more efficiently than does mA3^{d}Δ5.

C57BL/6-derived mAPOBEC3 restricts F-MuLV replication in the absence of the deaminase catalytic site. The above-

TABLE 2. Sequence variations of F-MuLV proviral genome observed for infected cells

Stable transfectant	Total no. of nucleotides analyzed[a]	No. of nucleotide exchanges[b]		
		G/A	C/T	Other mutations
FLAG	94,429	0	3	6
GFP	101,856	0	2	6
mA3^{h}Δ5	96,551	3	2	9
mA3^{d}	94,429	5[c]	0	5
mA3^{d}Δ5	90,185	3	2	5
hAPOBEC3G	95,490	55[d]	5	11
hAPOBEC3F	97,612	2	0	6

[a] A 1,061-nucleotide fragment between the U3 and *gag* sequences from the F-MuLV proviral DNA was cloned, and its sequence was analyzed for at least 90 clones.

[b] The entire contingency table was analyzed for the possible presence of group-wise difference, which indicated a P value of <0.001. An individual group-wise difference was then analyzed by Fisher's exact test.

[c] $P = 0.026$ in comparison with that of GFP but was not significant in comparison with that of FLAG.

[d] $P = 5.77 \times 10^{-17}$ in comparison with the data for FLAG, 4.55×10^{-18}, in comparison with that of GFP.

described results indicate that the major difference between the efficacies of the C57BL/6- and BALB/c-derived mAPOBEC3 proteins in restricting F-MuLV infection in vitro likely stems from the differences in their amino acid sequences (Fig. 1). To analyze this, we constructed reciprocal chimeras between mA3^{h}Δ5 and mA3^{d}Δ5 by mutually exchanging the N-terminal portion at ^{194}Q (Fig. 1) and established BALB/3T3 lines stably expressing the chimeric mAPOBEC3 (Fig. 3A). The progeny virus produced from the cells expressing the chimeric mA3^{d}Δ5/mA3^{h}Δ5 protein, with its N-terminal portion encoded by the BALB/c-derived *mA3^{d}*, failed to fully restrict F-MuLV replication, while the reciprocal mA3^{h}Δ5/mA3^{d}Δ5 construct restricted F-MuLV replication as efficiently as mA3^{h}Δ5 did (Fig. 3B). These results clearly localized the strain-dependent functional difference of mAPOBEC3Δ5 to the N-terminal portion harboring the CDD1.

It is not clear to what extent APOBEC3 proteins restrict retroviral integration through their deaminase activity as opposed to through a deaminase-independent mechanism (1, 4, 38, 39, 43). Sequencing of the multiple proviral genomes revealed a significant increase in G-to-A mutations in the *Mus dunni* cells infected with F-MuLV produced from the hAPOBEC3G-expressing cells (Table 2). Surprisingly, the proviruses cloned from the indicator cells infected with F-MuLV produced from the mA3^{h}Δ5-expressing cells did not show such a significant increase in G-to-A mutations in comparison with those observed for the cells infected with the control viruses. To further determine if the deaminase activity is required for the observed restriction of F-MuLV replication by mA3^{h}Δ5, mutations were introduced into its catalytic sites. mAPOBEC3, as well as hAPOBEC3G and hAPOBEC3F, harbors two CDD, of which only CDD2 is catalytically active in hAPOBEC3G (37, 38), while CDD1 is active in mAPOBEC3 (15). Mutation of the glutamic acid to alanine at position 73 (E73A) within CDD1, but not the equivalent mutation (E257A) within CDD2, abrogates mAPOBEC3 deaminase activity, as well as antiviral restriction, against *vif*-deficient HIV (15). We introduced these point mutations either individually or in combination into mA3^{h}Δ5 and generated stable transfectants in BALB/3T3 cells (Fig. 3C). The F-MuLV progeny viruses produced from all the mutant mA3^{h}Δ5 transfectants had reduced replicative activities in *Mus dunni* cells (Fig. 3D) in comparison with the virus produced from the control cells, regardless of the introduced mutation(s) into mAPOBEC3, although the E73A mutant showed a slightly reduced repressive activity, implicating some role for this catalytic site. These results, along with the lack of an evident increase in G-to-A substitutions in the integrated proviral genome (Table 2), indicate that mA3^{h}Δ5 may restrict F-MuLV replication in a deaminase-independent fashion.

C57BL/6-derived mAPOBEC3 restricts F-MuLV replication in vivo. The reduced infectivity of the progeny F-MuLV produced from the stably transfected cell lines might have resulted from an excessive amount of mAPOBEC3 protein that was forcibly incorporated into the virion. To examine directly the possible physiological effect of the putative resistant allele, *mA3^{b}*, on F-MuLV infection in vivo, we introduced the targeted disruption of the *APOBEC3* gene (31) into C57BL/6 mice by backcrossing. The progenies of heterozygous breeding pairs were genotyped (Fig. 4A), and the expression or lack of expression of the *mA3^{b}* allele in the spleen and bone marrow was confirmed by RT-PCR (Fig. 4B). Infectious center assays revealed that C57BL/6 mice deficient in mAPOBEC3 possessed nearly 100-fold higher numbers of F-MuLV-producing cells at postinfection day (PID) 6, both in the spleen and bone marrow, in comparison with that of the wild-type or heterozygous counterparts (Fig. 4C). To further determine if the allelic difference in the *APOBEC3* locus influences resistance to F-MuLV infection, heterozygous C57BL/6 *mA3$^{b/-}$* mice were mated with BALB/c mice, and the resultant CB6F$_1$ mice were genotyped and infected with F-MuLV. As expected, CB6F$_1$ mice of the *mA3$^{d/-}$* genotype expressed low levels of the full-length, as well as the short mAPOBEC3, mRNA in the bone marrow, while the *mA3$^{d/b}$* mice expressed a higher level of the mA3^{h}Δ5 message along with a low level of the full-length mA3^{d} mRNA (Fig. 4D). Importantly, *mA3$^{d/-}$* mice deficient in the C57BL/6-derived APOBEC3 protein harbored more than 100-times-larger numbers of F-MuLV-producing cells in their bone marrow than the wild-type *mA3$^{d/b}$* mice at PID 6, despite the expression of the BALB/c-derived *mA3^{d}* allele (Fig. 4E). Thus, the C57BL/6-derived *mA3^{b}* allele dominantly confers resistance to F-MuLV infection in the presence of the *mA3^{d}* allele.

C57BL/6-derived mAPOBEC3 restricts erythroid cell proliferation in mice infected with the pathogenic FV complex. To further determine if the *mA3^{b}* allele physiologically functions in conferring resistance to FV-induced pathogenesis, FV-susceptible CB6F$_1$ mice possessing or lacking the *mA3^{b}* allele were infected with FV. CB6F$_1$ *mA3$^{d/b}$* mice possessed on average 13.1% ± 9.2% gp70-positive (gp70^{+}) cells in their bone marrow at PID 7 (Fig. 4F), a large majority of which belonged to the TER119^{-} erythroblast population (25). On the other hand, when CB6F$_1$ mice lacking the *mA3^{b}* allele were infected with FV, significantly increased numbers (35.6% ± 11.9%, P = 0.00015) of bone marrow cells became positive for gp70, and these included more immature TER-119 cells. Reflecting the above differences, CB6F$_1$ *mA3$^{d/-}$* mice uniformly possessed extremely high hematocrit values at PID 21, while hematocrit

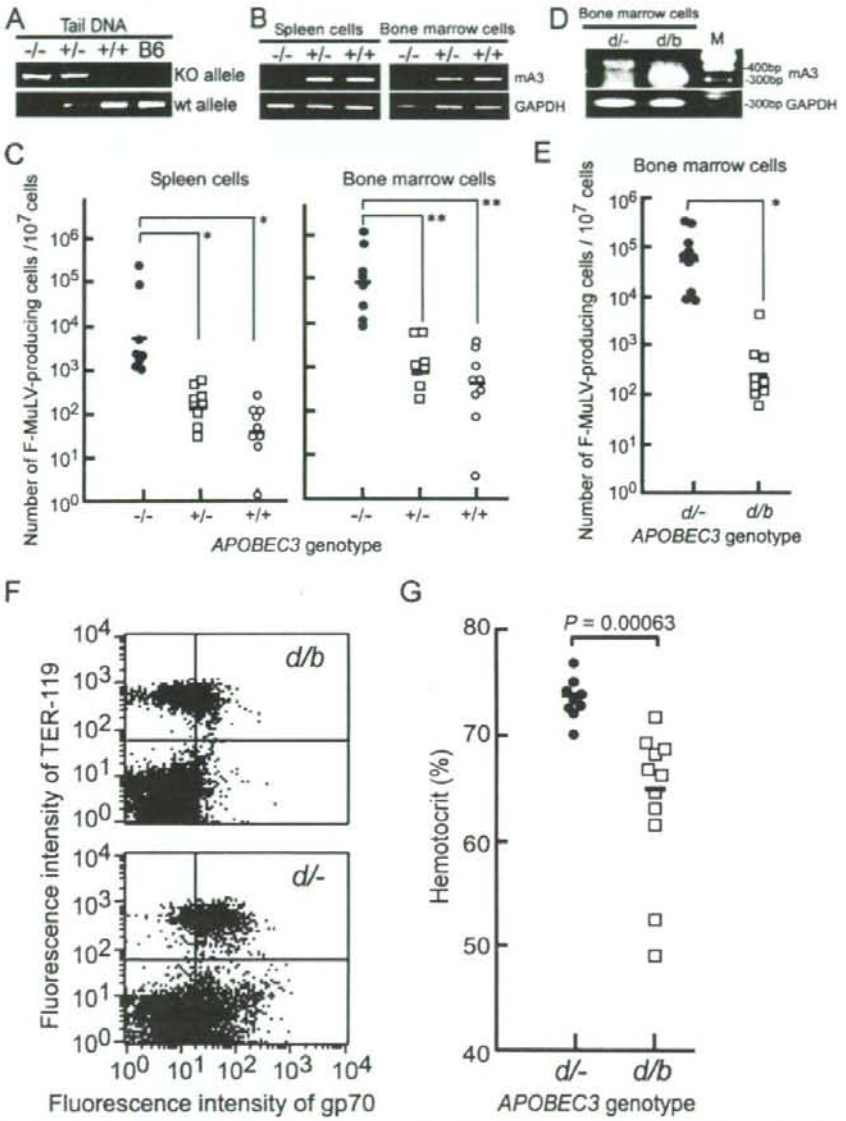

FIG. 4. Replication of F-MuLV in mAPOBEC3-deficient mice and the development of FV-induced disease in vivo. (A) Representative results for genotyping of the *APOBEC3* alleles by PCR. (B) Expression of mAPOBEC3 mRNA in the bone marrow and spleen of the APOBEC3-deficient C57BL/6 mice analyzed by RT-PCR is shown. (C) C57BL/6 mice possessing either the *APOBEC3*$^{-/-}$ (−/−) (n = 8), +/− (n = 10), or +/+ (n = 9) alleles were inoculated intravenously with 10^5 FFU of purified F-MuLV. F-MuLV infectious centers were enumerated on *Mus dunni* cells with anti-gp70 MAb on PID 6. Short horizontal bars indicate the means. *, $P < 0.02$; **, $P < 0.002$. (D) Expression of APOBEC3 mRNA in mAPOBEC3-deficient $CB6F_1$ mice analyzed by RT-PCR. (E) $CB6F_1$ mice possessing either the *APOBEC3*$^{d/-}$ (d/−) (n = 10) or d/b (n = 10) alleles were inoculated intravenously with 10^4 FFU of purified F-MuLV. F-MuLV infectious centers in the bone marrow were enumerated by coculturing *Mus dunni* cells and staining with anti-gp70 MAb on PID 6. Short horizontal bars indicate the means. The difference between the groups was analyzed by Student's t test: *, $P < 1 \times 10^{-7}$. (F and G) $CB6F_1$ mice possessing either the *APOBEC3*$^{d/-}$ (d/−) or d/b alleles were inoculated intravenously with 150 spleen FFU of FV complex. On PID 7, the cells prepared from the bone marrow were stained for TER119 and gp70 and were analyzed by flow cytometry (F). Five mice of each genotype were examined to calculate the means described in the text, and the dot graphs shown are of representative animals. On PID 21, hematocrit values were determined in the peripheral blood (G).

values for the *mA3*$^{r/h}$ mice were significantly lower (Fig. 4G). Thus, the *mA3*^{h} allele does confer resistance to FV-induced erythroid pathology.

DISCUSSION

It has been generally accepted that retroviruses have evolved to evade the antiviral activities of their natural host's APOBEC proteins. In fact, primate lentiviruses counter the action of primate A3G with their Vif protein, while Vif is unable to counteract mAPOBEC3 and HIV-1 is highly susceptible to restriction by mAPOBEC3 (28, 42). The primate APOBEC3G gene predates HIV-related lentiviruses and has been under strong selective pressure for its conserved functionality (41). Thus, physiological targets of primate APOBEC3G might be endogenous retroviruses and nonautonomous retroelements (10, 14). Similarly, MuLV has also evolved mechanisms to block mAPOBEC3. These include the competitive exclusion of mAPOBEC3 from MuLV particles (1, 13), cleavage of virion-incorporated mAPOBEC3 by viral protease (1), and inhibition of the deaminase activity (4). However, possible inhibitory roles of APOBEC3 proteins on exogenous retroviral infection in vivo have become evident through the study of human lentiviruses. Thus, the patterns of hypermutation of HIV from infected individuals have indicated that the hAPOBEC3 proteins fulfill an inhibitory role (2, 26), and the levels of hAPOBEC3G expression have been associated with suppression of HIV-1 viremia and HIV-1-exposed but -uninfected status (3, 20). Regarding the mouse, however, the only previously demonstrated target for mAPOBEC3 in vivo was the betaretrovirus MMTV, with mAPOBEC3-deficient mice giving increased viral replication (39). Although putatively residual activities exerted by mAPOBEC3Δ5 in inhibiting MuLV integration have been reported (1, 4), these might have been caused by an excessive amount of mAPOBEC3 protein forcibly incorporated into the virion, especially when the experiments were performed by transfecting MuLV packaging cells with an mAPOBEC3-expressing plasmid vector.

Based on our previous demonstration that the FV resistance gene *Rfv3* colocalized with the *APOBEC3* locus (23, 36), we have shown here that the mouse gammaretrovirus F-MuLV is a target for mAPOBEC3 and, further, that mAPOBEC3 acts to restrict viral pathogenesis in vivo (Fig. 4). Gammaretroviruses have coevolved with their natural hosts (48), with MuLV and related endogenous retroviruses distributed more widely than MMTV among murine strains and species. Nevertheless, C57BL/6 and closely related C57BL/10 (B10) mice possess multiple host factors that make these strains resistant to FV-induced disease development (5, 22, 32, 36). We have shown in the present paper that differences in the sequence of mAPOBEC3 (Fig. 1), along with different expression levels in the hematopoietic tissues (Fig. 2A to C) account for part of this polymorphism. Further, we have also localized the functional difference between F-MuLV-restricting mA3^{h}Δ5 and less-restricting mA3^{d}Δ5 to the N-terminal portion other than the deaminase catalytic site (Fig. 3). Thus, F-MuLV infection in mice may not only provide a tractable model for the study of the in vivo mechanism of APOBEC3-mediated retroviral restriction, it may also provide insight into mechanisms of virus-host coevolution.

Finally, whether or not the *Rfv3* locus is identical to the *APOBEC3* locus must be discussed. The *Rfv3* gene was first described by comparing the persistence of viremia after FV infection between the prototypic FV-resistant B10.A/SgSn and the susceptible A/WySn mice that share the same *H-2*^{a} haplotype (6). A/WySn mice remained viremic at more than 30 days after FV infection, while B10.A/SgSn mice had cleared viremia by PID 30. Since F_1 crosses between these two strains were not viremic and about half of the (B10.A × A/WySn) × A/WySn backcross mice showed viremia at PID 30, the presence of a recessive host gene in A/WySn mice was postulated in association with the persistence of viremia and was designated the *Rfv3*^{s} allele. Thus, B10.A/SgSn mice possess a dominant allele, the *Rfv3*^{r}, conferring the early clearance of viremia. The *Rfv3* locus was later mapped to within chromosome 15 (17, 47). As we have shown here (Fig. 1), B10.A/SgSn mice share the *APOBEC3* sequence with C57BL/6 and A/WySn with BALB/c. Therefore, it is conceivable that the FV-restricting *mA3*^{h} allele in B10.A/SgSn mice functioned to limit the replication of FV and thus contributed to the observed earlier clearance of viremia. However, for the clearance of viremia in FV-infected mice, the host immune responses are also required. In fact, B-cell-deficient C57BL/6 mice possessed higher levels of viremia than their wild-type counterparts at PID 7 (30), and FV-producing cells in the bone marrow and spleen could not be eliminated, even after effective priming of T cells with the viral antigens, in the absence of Ab-producing cells (24, 30). Thus, although the *mA3*^{h} allele does contribute to the reduction in the number of virus-producing cells in the early stage of FV infection (Fig. 4), it must influence the immune responses, either directly or indirectly, to explain the phenotypes influenced by the *Rfv3* gene. In this regard, (B10.A × A/WySn)F_1 mice do produce F-MuLV-neutralizing Ab earlier than A/WySn mice do (23). The less massive expansion of FV-infected erythroid cells in the *mA3*^{h}-possessing mice than in those lacking this resistant genotype (Fig. 4) might result in the possible preservation of the stromal architecture that is required for cell-to-cell interactions involved in lymphocyte priming and B-cell activation. Further studies are required to clarify the presumable identity of the mouse *APOBEC3* gene as the *Rfv3* gene.

ACKNOWLEDGMENTS

This work was supported in part by grants-in-aid for scientific research from the Ministry of Education, Culture, Sports, Science and Technology of Japan, including the High-Tech Research Center project, and grants from the Ministry of Health, Labor and Welfare of Japan, the Japan Health Sciences Foundation, and the Naito Foundation.

We thank J. B. Dowell for critical readings and corrections of the manuscript.

REFERENCES

1. **Abudu, A., A. Takaori-Kondo, T. Izumi, K. Shirakawa, M. Kobayashi, A. Sasada, K. Fukunaga, and T. Uchiyama.** 2006. Murine retrovirus escapes from murine APOBEC3 via two distinct novel mechanisms. Curr. Biol. **16**:1565–1570.
2. **Beale, R. C., S. K. Petersen-Mahrt, I. N. Watt, R. S. Harris, C. Rada, and M. S. Neuberger.** 2004. Comparison of the differential context-dependence of DNA deamination by APOBEC enzymes: correlation with mutation spectra *in vivo*. J. Mol. Biol. **337**:585–596.
3. **Biasin, M., L. Piacentini, S. Lo Caputo, Y. Kanari, G. Magri, D. Trabattoni, V. Naddeo, L. Lopalco, A. Clivio, E. Cesana, F. Fasano, C. Bergamaschi, F. Mazzotta, M. Miyazawa, and M. Clerici.** 2007. Apolipoprotein B mRNA-

editing enzyme, catalytic polypeptide-like 3G: a possible role in the resistance to HIV of HIV-exposed seronegative individuals. J. Infect. Dis. **195:** 960–964.
4. **Browne, E. P., and D. R. Littman.** 2008. Species-specific restriction of Apobec3-mediated hypermutation. J. Virol. **82:**1305–1313.
5. **Chesebro, B., M. Miyazawa, and W. J. Britt.** 1990. Host genetic control of spontaneous and induced immunity to Friend murine retrovirus infection. Annu. Rev. Immunol. **8:**477–499.
6. **Chesebro, B., and K. Wehrly.** 1979. Identification of a non-H-2 gene (Rfv-3) influencing recovery from viremia and leukemia induced by Friend virus complex. Proc. Natl. Acad. Sci. USA **76:**425–429.
7. **Chesebro, B., K. Wehrly, M. Cloyd, W. Britt, J. Portis, J. Collins, and J. Nishio.** 1981. Characterization of mouse monoclonal antibodies specific for Friend murine leukemia virus-induced erythroleukemia cells: Friend-specific and FMR-specific antigens. Virology **112:**131–144.
8. **Chiu, Y. L., and W. C. Greene.** 2006. Multifaceted antiviral actions of APOBEC3 cytidine deaminases. Trends Immunol. **27:**291–297.
9. **Chiu, Y. L., V. B. Soros, J. F. Kreisberg, K. Stopak, W. Yonemoto, and W. C. Greene.** 2005. Cellular APOBEC3G restricts HIV-1 infection in resting $CD4^+$ T cells. Nature **435:**108–114.
10. **Chiu, Y. L., H. E. Witkowska, S. C. Hall, M. Santiago, V. B. Soros, C. Esnault, T. Heidmann, and W. C. Greene.** 2006. High-molecular-mass APOBEC3G complexes restrict Alu retrotransposition. Proc. Natl. Acad. Sci. USA **103:**15588–15593.
11. **Conticello, S. G., R. S. Harris, and M. S. Neuberger.** 2003. The Vif protein of HIV triggers degradation of the human antiretroviral DNA deaminase APOBEC3G. Curr. Biol. **13:**2009–2013.
12. **Delebecque, F., R. Suspene, S. Calattini, N. Casartelli, A. Saib, A. Froment, S. Wain-Hobson, A. Gessain, J. P. Vartanian, and O. Schwartz.** 2006. Restriction of foamy viruses by APOBEC cytidine deaminases. J. Virol. **80:**605–614.
13. **Doehle, B. P., A. Schafer, H. L. Wiegand, H. P. Bogerd, and B. R. Cullen.** 2005. Differential sensitivity of murine leukemia virus to APOBEC3-mediated inhibition is governed by virion exclusion. J. Virol. **79:**8201–8207.
14. **Esnault, C., O. Heidmann, F. Delebecque, M. Dewannieux, D. Ribet, A. J. Hance, T. Heidmann, and O. Schwartz.** 2005. APOBEC3G cytidine deaminase inhibits retrotransposition of endogenous retroviruses. Nature **433:**430–433.
15. **Hakata, Y., and N. R. Landau.** 2006. Reversed functional organization of mouse and human APOBEC3 cytidine deaminase domains. J. Biol. Chem. **281:**36624–36631.
16. **Harris, R. S., K. N. Bishop, A. M. Sheehy, H. M. Craig, S. K. Petersen-Mahrt, I. N. Watt, I. N., M. S. Neuberger, and M. H. Malim.** 2003. DNA deamination mediates innate immunity to retroviral infection. Cell **113:**803–809.
17. **Hasenkrug, K. J., A. Valenzuela, V. A. Letts, J. Nishio, B. Chesebro, and W. N. Frankel.** 1995. Chromosome mapping of Rfv3, a host resistance gene to Friend murine retrovirus. J. Virol. **69:**2617–2620.
18. **Iwanami, N., A. Niwa, Y. Yasutomi, N. Tabata, and M. Miyazawa.** 2001. Role of natural killer cells in resistance against friend retrovirus-induced leukemia. J. Virol. **75:**3152–3163.
19. **Jern, P., J. P. Stoye, and J. M. Coffin.** 2007. Role of APOBEC3 in genetic diversity among endogenous murine leukemia viruses. PLoS Genet. **3:**2014–2022.
20. **Jin, X., A. Brooks, H. Chen, R. Bennett, R. Reichman, and H. Smith.** 2005. APOBEC3G/CEM15 (hA3G) mRNA levels associate inversely with human immunodeficiency virus viremia. J. Virol. **79:**11513–11516.
21. **Jonsson, S. R., R. S. LaRue, M. D. Stenglein, S. C. Fahrenkrug, V. Andresdottir, and R. S. Harris.** 2007. The restriction of zoonotic PERV transmission by human APOBEC3G. PLoS ONE **2:**e893.
22. **Kabat, D.** 1989. Molecular biology of Friend viral erythroleukemia. Curr. Top. Microbiol. Immunol. **148:**1–42.
23. **Kanari, Y., M. Clerici, H. Abe, H. Kawabata, D. Trabattoni, S. Lo Caputo, F. Mazzotta, H. Fujisawa, A. Niwa, C. Ishihara, Y. A. Takei, and M. Miyazawa.** 2005. Genotypes at chromosome 22q12-13 are associated with HIV-1-exposed but uninfected status in Italians. AIDS **19:**1015–1024.
24. **Kawabata, H., A. Niwa, S. Tsuji-Kawahara, H. Uenishi, N. Iwanami, H. Matsukuma, H. Abe, N. Tabata, H. Matsumura, and M. Miyazawa.** 2006. Peptide-induced immune protection of $CD8^+$ T cell-deficient mice against Friend retrovirus-induced disease. Int. Immunol. **18:**183–198.
25. **Kina, T., K. Ikuta, E. Takayama, K. Wada, A. S. Majumdar, I. L. Weissman, and Y. Katsura.** 2000. The monoclonal antibody TER-119 recognizes a molecule associated with glycophorin A and specifically marks the late stages of murine erythroid lineage. Br. J. Haematol. **109:**280–287.
26. **Liddament, M. T., W. L. Brown, A. J. Schumacher, and R. S. Harris.** 2004. APOBEC3F properties and hypermutation preferences indicate activity against HIV-1 in vivo. Curr. Biol. **14:**1385–1391.
27. **Mangeat, B., P. Turelli, G. Caron, M. Friedli, L. Perrin, and D. Trono.** 2003. Broad antiretroviral defense by human APOBEC3G through lethal editing of nascent reverse transcripts. Nature **424:**99–103.
28. **Mariani, R., D. Chen, B. Schrofelbauer, F. Navarro, R. Konig, B. Bollman, C. Munk, H. Nymark-McMahon, and N. R. Landau.** 2003. Species-specific exclusion of APOBEC3G from HIV-1 virions by Vif. Cell **114:**21–31.
29. **Marin, M., K. M. Rose, S. L. Kozak, and D. Kabat.** 2003. HIV-1 Vif protein binds the editing enzyme APOBEC3G and induces its degradation. Nat. Med. **9:**1398–1403.
30. **Messer, R. J., U. Dittmer, K. E. Peterson, and K. J. Hasenkrug.** 2004. Essential role for virus-neutralizing antibodies in sterilizing immunity against Friend retrovirus infection. Proc. Natl. Acad. Sci. USA **101:**12260–12265.
31. **Mikl, M. C., I. N. Watt, M. Lu, W. Reik, S. L. Davies, M. S. Neuberger, and C. Rada.** 2005. Mice deficient in APOBEC2 and APOBEC3. Mol. Cell. Biol. **25:**7270–7277.
32. **Miyazawa, M.** 2004. Host genes that influence immune and non-immune resistance mechanisms against retroviral infections. Rec. Res. Dev. Immunol. **6:**105–118.
33. **Miyazawa, M., J. Nishio, and B. Chesebro.** 1988. Genetic control of T cell responsiveness to the Friend murine leukemia virus envelope antigen. Identification of class II loci of the H-2 as immune response genes. J. Exp. Med. **168:**1587–1605.
34. **Miyazawa, M., J. Nishio, K. Wehrly, and B. Chesebro.** 1992. Influence of MHC genes on spontaneous recovery from Friend retrovirus-induced leukemia. J. Immunol. **148:**644–647.
35. **Miyazawa, M., J. Nishio, K. Wehrly, C. S. David, and B. Chesebro.** 1992. Spontaneous recovery from Friend retrovirus-induced leukemia. Mapping of the *Rfv-2* gene in the Q/TL region of mouse MHC. J. Immunol. **148:**1964–1967.
36. **Miyazawa, M., S. Tsuji-Kawahara, and Y. Kanari.** 2008. Host genetic factors that control immune responses to retrovirus infections. Vaccine **26:**2981–2996.
37. **Navarro, F., B. Bollman, H. Chen, R. Konig, Q. Yu, K. Chiles, and N. R. Landau.** 2005. Complementary function of the two catalytic domains of APOBEC3G. Virology **333:**374–386.
38. **Newman, E. N., R. K. Holmes, H. M. Craig, K. C. Klein, J. R. Lingappa, M. H. Malim, and A. M. Sheehy.** 2005. Antiviral function of APOBEC3G can be dissected from cytidine deaminase activity. Curr. Biol. **15:**166–170.
39. **Okeoma, C. M., N. Lovsin, B. M. Peterlin, and S. R. Ross.** 2007. APOBEC3 inhibits mouse mammary tumour virus replication in vivo. Nature **445:**927–930.
40. **Robertson, M. N., M. Miyazawa, S. Mori, B. Caughey, L. H. Evans, S. F. Hayes, and B. Chesebro.** 1991. Production of monoclonal antibodies reactive with a denatured form of the Friend murine leukemia virus gp70 envelope protein: use in a focal infectivity assay, immunohistochemical studies, electron microscopy and western blotting. J. Virol. Methods **34:**255–271.
41. **Sawyer, S. L., M. Emerman, and H. S. Malik.** 2004. Ancient adaptive evolution of the primate antiviral DNA-editing enzyme APOBEC3G. PLoS Biol. **2:**e275.
42. **Schrofelbauer, B., Q. Yu, and N. R. Landau.** 2004. New insights into the role of Vif in HIV-1 replication. AIDS Rev. **6:**34–39.
43. **Shindo, K., A. Takaori-Kondo, M. Kobayashi, A. Abudu, K. Fukunaga, and T. Uchiyama.** 2003. The enzymatic activity of CEM15/Apobec-3G is essential for the regulation of the infectivity of HIV-1 virion but not a sole determinant of its antiviral activity. J. Biol. Chem. **278:**44412–44416.
44. **Sitbon, M., B. Sola, L. Evans, J. Nishio, S. F. Hayes, K. Nathanson, C. F. Garon, and B. Chesebro.** 1986. Hemolytic anemia and erythroleukemia, two distinct pathogenic effects of Friend MuLV: mapping of the effects to different regions of the viral genome. Cell **47:**851–859.
45. **Stopak, K., C. de Noronha, W. Yonemoto, and W. C. Greene.** 2003. HIV-1 Vif blocks the antiviral activity of APOBEC3G by impairing both its translation and intracellular stability. Mol. Cell **12:**591–601.
46. **Sugahara, D., S. Tsuji-Kawahara, and M. Miyazawa.** 2004. Identification of a protective $CD4^+$ T-cell epitope in $p15^{gag}$ of Friend murine leukemia virus and role of the MA protein targeting the plasma membrane in immunogenicity. J. Virol. **78:**6322–6334.
47. **Super, H. J., K. J. Hasenkrug, S. Simmons, D. M. Brooks, R. Konzek, K. D. Sarge R. I. Morimoto, N. A. Jenkins, D. J. Gilbert, N. G. Copeland, W. Frankel, and B. Chesebro.** 1999. Fine mapping of the friend retrovirus resistance gene, *Rfv3*, on mouse chromosome 15. J. Virol. **73:**7848–7852.
48. **Tomonaga, K., and J. M. Coffin.** 1999. Structures of endogenous nonecotropic murine leukemia virus (MLV) long terminal repeats in wild mice: implication for evolution of MLVs. J. Virol. **733:**4327–4340.
49. **Yu, X., Y. Yu, B. Liu, K. Luo, W. Kong, P. Mao, and X. F. Yu.** 2003. Induction of APOBEC3G ubiquitination and degradation by an HIV-1 Vif-Cul5-SCF complex. Science **302:**1056–1060.